



CHALMERS



Gravitational instabilities in nearby star-forming galaxies

A study of localized structures in spiral galaxies

Master's thesis in Physics & Astronomy

Madeleine Yttergren
Supervisor: Alessandro Romeo

MASTER'S THESIS

Gravitational instabilities in nearby star-forming galaxies

A study of localized structures in spiral galaxies

Madeleine Yttergren
Supervisor: Alessandro Romeo



CHALMERS
UNIVERSITY OF TECHNOLOGY

Department of Earth and Space Sciences
CHALMERS UNIVERSITY OF TECHNOLOGY
Gothenburg, Sweden

June 2016

Gravitational instabilities in nearby star-forming galaxies
A study of localized structures in spiral galaxies
Madeleine Yttergren, m.yttergren@gmail.com

© MADELEINE YTTERGREN, 2016.

Department of Earth and Space Sciences
Chalmers University of Technology
SE-412 96 Gothenburg, Sweden
+46 31-772 1000

Onsala Space Observatory
SE-439 92 Onsala, Sweden
+46 31-772 5500

Cover: A composite image of NGC 3627, note the distinct spiral arms and bar.
Source: <https://www.eso.org/public/images/eso0338c/>.

Typeset in L^AT_EX
Gothenburg, Sweden 2016

Gravitational instabilities in nearby star-forming galaxies

A study of localized structures in spiral galaxies

Madeleine Yttergren

Department of Earth and Space Sciences

Chalmers University of Technology

Abstract

The dynamics of nearby star-forming galaxies has long intrigued and eluded scientists. Gravitational instabilities are one of the engines of star formation and "hidden" structures in spiral galaxies, such as bars within bars, ovals and nuclear rings. The radial locations and extent of star-forming regions and other structures can be analysed using the multi-component Q stability parameter of Romeo & Falstad (2013). This parameter accounts for a disc constituted of multiple components, as well as for disc thickness. In this thesis we study the gravitational instabilities of nearby star-forming spiral galaxies focusing on three disc components (atomic hydrogen, molecular hydrogen and stars), as well as their dynamical interplay. We also use another disc instability diagnostic, the characteristic instability wavelength (Romeo & Falstad, 2013), which predicts the sizes of the regions prone to instabilities. Together with the Q stability parameter, we thereby have an appropriate method for analysing galactic discs.

We use observational data from four high-quality surveys: THINGS, HERACLES, BIMA SONG and SINGS, which were first analysed and modelled by Leroy et al. (2008). We discover a new ability of the characteristic instability wavelength: the ability to accurately predict the transition between the components dominating the instability. Our analysis also illustrates that the use of higher-resolution data and more accurate modelling, together with the Romeo & Falstad (2013) disc instability diagnostic, may reveal a wider variety of hidden structures in nearby star-forming galaxies.

Keywords: gravitational instabilities, ISM:kinematics and dynamics, galaxies:spiral, galaxies:kinematics and dynamics, galaxies:structure.

Acknowledgements

First and foremost I want to express my eternal gratitude to my supervisor, Alessandro Romeo. For his ever-present and invaluable support and feedback, concerning both the work presented here as well as my future carrier. The work throughout this project has been truly rewarding, and the end-result would not have reached the same level without his guidance and vast wisdom.

I also want to acknowledge the great work of my opponents, Filippa Hallqvist and Axel Widmark. By giving me their time they provided insightful comments, ideas and questions. I want to thank Filippa for her enthusiasm as she decided to be my opponent, and for all the inspiring discussions throughout our studies together.

In addition, I am grateful for the enthusiasm of Robert Freiholtz, for his ever-present hope that I would get stuck in MATLAB, so he could rescue me.

Lastly, I would like to express my gratitude for the time spent at Onsala Space Observatory. The relaxed and welcoming atmosphere, the meetings and the seminars have been very motivating, and have made sure to inspire me any time I felt low.

Madeleine Yttergren, Gothenburg, May 2016



Contents

1	Introduction	1
2	Background	3
2.1	Spiral galaxies and resonances	3
2.2	Gravitational instability	4
2.2.1	The classical Toomre parameter	5
2.2.2	The effect of disc thickness	5
2.2.3	Two components: stars and gas	6
2.2.4	Wang-Silk approximation	6
2.2.5	Romeo-Falstad instability parameter for multicomponent discs	6
2.2.6	The characteristic instability wavelength	7
2.3	Observational background	7
2.3.1	Leroy et al. (2008): data and modelling	8
3	Results & Discussion	9
3.1	The whole sample of THINGS spirals	9
3.1.1	The stability parameter	9
3.1.2	The characteristic instability wavelength	11
3.1.3	Correlation with the mass distribution	12
3.2	Is there a relation between the characteristic instability wavelength and local structures in galactic discs?	14
3.2.1	A case study: NGC 6946	14
3.2.2	NGC 3351	15
3.2.3	NGC 7331	18
3.2.4	NGC 3627	18
3.2.5	NGC 628	20
3.2.6	Any other features?	22
3.3	Discussion	23
3.3.1	Progress in the field	23
4	Conclusions	25
	References	27
A	Is the short-wavelength approximation satisfied?	I
B	Radial profiles for other spiral galaxies	III

1

Introduction

Observations of nearby spiral galaxies show extensive star formation. Star formation is a vital aspect of the evolution of galaxies, and is connected to the composition of the interstellar medium, stellar feedback, as well as a number of other factors, some of which are still unclear. Despite being of vast importance, the process of forming a star is poorly understood. One of the engines involved in star formation is gravitational instabilities. Gravitational instabilities promote local gravitational collapse/fragmentation in the interstellar medium, and thereby encourage the formation of a star. The phenomenon of gravitational instability and the models describing them are highly complex. Simpler models can be deduced by limiting the number of processes and components included.

The most commonly used diagnostic has been the classical Safronov-Toomre stability criterion (Safronov, 1960; Toomre, 1964): $Q > 1$, where the Q parameter depends on the rotation curve of the galaxy, as well as on the surface density and the velocity dispersion of the disc. The main limitation of this criterion is that it applies to an infinitesimally thin disc of either gas or stars, while both components generally contribute to gravitational instability (Lin & Shu, 1966; Jog & Solomon, 1984a,b). Fortunately, through the analyses of Bertin & Romeo (1988), Elmegreen (1995), Jog (1996), Rafikov (2001), Romeo & Wiegert (2011) and Romeo & Falstad (2013) amongst others, the work continued to encompass discs of multiple components. The Q stability parameter of Romeo & Falstad (2013) is easy to use and can account for multiple disc components as well as disc thickness. In addition, this Q parameter indicates which disc component dominates the instability.

Aside from the Q stability parameter of Romeo & Falstad (2013), there is another useful and powerful diagnostic for studying gravitational instabilities: the characteristic instability wavelength, λ , which can predict the sizes of regions prone to collapse/fragmentation. This novel parameter has recently been used to study three star-forming spiral galaxies: NGC 1068 (Romeo & Fathi, 2016), NGC 6946 (Romeo & Fathi, 2015) and NGC 7469 (Fathi et al., 2015), with promising results. The characteristic instability wavelength has shown the ability to reveal "hidden" structures in galactic discs, such as bars within bars, as well as nuclear spirals and rings, which are generally difficult to identify. Compared to other diagnostics, the characteristic instability wavelength is a simpler, easier-to-apply and more accurate diagnostic.

This thesis is devoted to a detailed analysis of gravitational instabilities in nearby star-forming galaxies, focusing on the characteristic instability wavelength. The aim is to explore the extent to which this simple diagnostic can be used to retrieve information regarding hidden structures in disc galaxies. A thorough stability analysis of 12 spiral galaxies is then carried out using both the characteristic instability

wavelength and the Q stability parameter.

The rest of the thesis is organised into three main chapters (and two appendices): Background (Chapter 2), Results & Discussion (Chapter 3) and Conclusions (Chapter 4), where each chapter begins with a short summary before turning to the details. Chapter 2 is devoted to diagnostics of gravitational instabilities. It begins with reviewing the classical Safronov-Toomre stability criterion and the Wang-Silk approximation, which is then extended to encompass multiple discs components and disc thickness through the Q stability parameter of Romeo & Falstad (2013). The last part of this chapter contains a description of the observational data and their modelling. The results of the application of the Q stability parameter and the characteristic instability wavelength on the whole sample of the 12 spiral galaxies are presented in Chapter 3. Besides, a more detailed analysis of 5 of the galaxies is carried out. The last part of this chapter entails a discussion focused on the importance of observed radial profiles and an account of the recent progress therein. The thesis is concluded in Chapter 4, with the most important insights and messages. In addition to the main chapters, the two appendices contain radial profiles of individual galaxies, as well as a validity check of our analysis.

2

Background

The study of galaxies and gravitational instabilities have a long history, and a certain amount of theoretical knowledge is preferred. The first half of this chapter is dedicated to a discussion of the theory and the models of gravitational instabilities, while the second half presents the surveys and the dataset used in the analyses within this thesis.

First, the simplest model of a one component infinitesimally thin disc is presented, together with a criterion predicting its stability: the Safronov-Toomre stability criterion. Thereafter we move on to thick discs and discs consisting of two or more components. We present a diagnostic for predicting the sizes of unstable regions: the characteristic instability wavelength. To begin, a brief introduction to the morphology of spiral galaxies and the importance of resonances in the galactic disc is provided.

2.1 Spiral galaxies and resonances

Spiral galaxies are disc galaxies with waves of enhanced density that forms spiral arms. Different structures can be present, such as bars, ovals and rings. Ovals have similar kinematic properties as bars but are more optically diffuse. To classify the spiral galaxies depending on their morphology, the Hubble classification scheme is most often adopted (see Fig. 2.1). The Hubble classification has been elaborated by de Vaucouleur into a more complete notation, where Kormendy (2013) aids in a brief summary of this extended notation:

- SA(s)a: a non-barred (A) tightly wound (a) spiral (S) galaxy.
- SB(r)c: a barred (B) loosely wound (c) spiral galaxy with a gaseous/stellar ring (r) (the ring is most often located outside the bar ends, from which the spiral arms origin).
- SAB(rs)ab: a galaxy with a weak bar (AB) and spiral arms rather tightly wound (ab), and a weak ring (rs).

The spiral arms transport energy away from the coherent rotational motion to cause an increase in the random velocity of stars, transporting angular momentum to outside of the corotation resonance. The corotation resonance is where the disc and the pattern/density wave move at the same speed. Kormendy & Kennicutt (2004) describe the conditions of the corotation resonance, the Lindblad resonances and the ultraharmonic 4:1 resonance for a bar/a two armed spiral¹, accordingly:

- The corotation resonance (CR): $\Omega(R) = \Omega_p$

¹If the galaxy has m arms, the term $\kappa/2$ becomes κ/m .

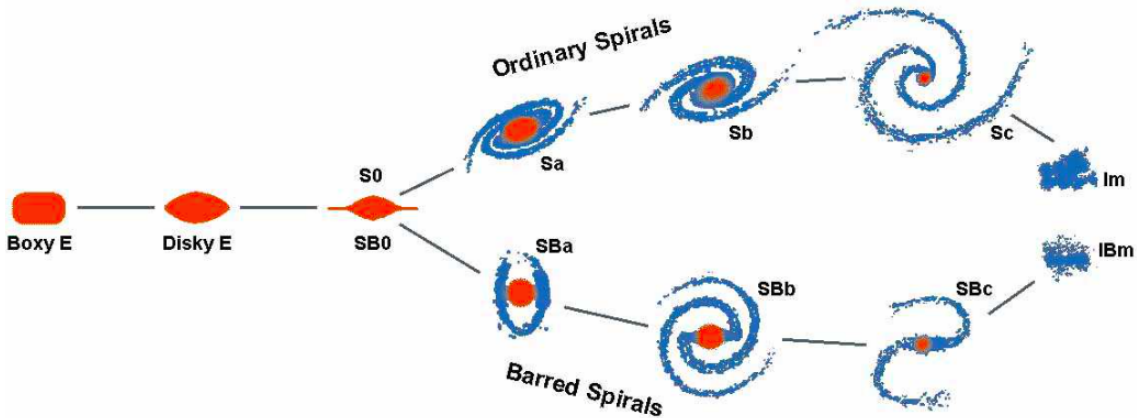


Figure 2.1: The Hubble Classification scheme, from Kormendy (2013). Early type galaxies to the left and late type galaxies to the right.

- The inner Lindblad resonance (ILR): $\Omega(R) - \kappa(R)/2 = \Omega_p$
- The outer Lindblad resonance (OLR): $\Omega(R) + \kappa(R)/2 = \Omega_p$
- The ultraharmonic 4:1 resonance (UHR): $\Omega(R) - \kappa(R)/4 = \Omega_p$,

where κ is the frequency of which a radially displaced particle oscillates, namely the epicyclic frequency.

Outside the CR, the gas is transported outwards towards the OLR. At the OLR the gas is collected and there is a possibility of forming a ring. Ring formation is possible and likely at a couple of other resonances as well. First and foremost it is at the ILR, which is situated at a radius where the pattern speed is smaller than the velocity of the disc. The gas located just inside the CR is transported towards the ILR, where it accumulates. If a galaxy has two ILRs, due to two different pattern speeds of two different structural components, the gas will gather at the inner ILR. Between the ILR and the CR the UHR is located. For example, in a galaxy where the ILR is located within the main bar a ring can form at the UHR instead.

The spiral arms are important in transporting gas inwards. To avoid the accumulation of gas at the Lindblad resonances (or UHR), resonance overlaps between different structures can occur. For example in a barred galaxy, if the ILR of the spiral structure coincides with the CR of the main bar (which is common since the speed of the bar often coincides with the speed of the ILR of the pattern (Kormendy, 2013)), the gas is effectively transported inward without accumulation.

2.2 Gravitational instability

For every wave that propagates there is a way to relate the wavenumber, k , and the frequency, ω . For a sound wave in vacuum this relation is simply: $\omega^2 = c_s^2 k^2$, where c_s is the sound speed. For a gravitational perturbation in a galactic disc this is somewhat more complicated.

Safronov (1960) considered a differentially rotating disc of negligible thickness, consisting solely of a fluid component, subject to axisymmetric perturbations (a perturbation that affects the galaxy in a cylindrically symmetric manner, only ra-

dially dependent). This culminated in an expression for a sound wave modified by gravity as a dispersion relation of the following form (Binney & Tremaine, 2008):

$$\omega^2 = \kappa^2 + \sigma^2 k^2 - 2\pi G \Sigma_0 k \quad (2.1)$$

where the first factor on the right hand side describes the stabilising effect of differential rotation, the second factor the stabilising effect due to random motions, and the last term entails the destabilising contribution of self-gravity. G is the gravitational constant, σ is the 1D velocity dispersion, κ is the epicyclic frequency and Σ_0 is the surface density.

If the right hand side of Eq. (2.1) is positive, $\omega^2 > 0$, the disc is stable. Deducing the minimum of Eq. (2.1) therefore provides a lower constraint on the wavenumber, corresponding to the maximum growth rate (see, e.g. Binney & Tremaine (2008)):

$$k = \frac{\pi G \Sigma_0}{\sigma^2} \quad (2.2)$$

2.2.1 The classical Toomre parameter

Eq. (2.2) together with $\omega^2 > 0$ and Eq. (2.1), results in the the Safronov-Toomre criterion for stability:

$$Q > 1, \quad \text{where} \quad Q = \frac{\sigma \kappa}{\pi G \Sigma_0}. \quad (2.3)$$

This expression is based on a number of assumptions: local (also called the short-wavelength approximation), linear and axisymmetric perturbations. If either one of these assumptions are violated, defining a stability criterion becomes highly non-trivial and the existence of such a criterion is not even generally accepted. For example, if the assumption of axisymmetric perturbations is relaxed, Romeo & Fathi (2015) state that a value of $Q > 2$ can be required to stabilise the system.

2.2.2 The effect of disc thickness

A factor that can increase the stability parameter is the effect of the thickness of the galactic disc. Romeo & Wiegert (2011) and Romeo & Falstad (2013) explain that the thickness of the disc acts in a stabilising manner providing a correction to the classical Safronov-Toomre parameter with a factor T . The effective stability parameter becomes TQ , where T is:

$$T = \begin{cases} 1 + 0.6 \left(\frac{\sigma_z}{\sigma_R} \right)^2 & \text{for } 0 \lesssim \sigma_z / \sigma_R \lesssim 0.5 \\ 0.8 + 0.7 \left(\frac{\sigma_z}{\sigma_R} \right) & \text{for } 0.5 \lesssim \sigma_z / \sigma_R \lesssim 1 \end{cases} \quad (2.4)$$

For a collisional component such as interstellar gas, the ratio of vertical to radial velocity dispersion is $\sigma_z / \sigma_R \approx 1$.

2.2.3 Two components: stars and gas

So far we have considered one collisional component, i.e. a fluid, but a galaxy is not made up out of only one component. The assumption of a collisional component is valid for the gas, but stars are not collisional. Fortunately Bertin & Romeo (1988), Rafikov (2001) and Romeo & Falstad (2013) showed that treating stars as a collisional component does not affect the stability criterion significantly.

2.2.4 Wang-Silk approximation

Wang & Silk (1994) proposed a manner of calculating the effective stability parameter for infinitesimally thin, two component, discs:

$$\frac{1}{Q} = \frac{1}{Q_*} + \frac{1}{Q_{gas}} \quad (2.5)$$

where Q_* is the classical Safronov-Toomre parameter for the stars, and Q_{gas} for the gas. This approximation is called the Wang-Silk approximation, and is based on the incorrect assumption of decoupled contribution to the instability from stellar and gaseous components (proven incorrect by Jog (1996)). Romeo & Wiegert (2011) calculated the typical error of this two component approximation, and discovered a significant under-estimation of the stability parameter.

2.2.5 Romeo-Falstad instability parameter for multicomponent discs

A rigorous stability analysis was carried out by Romeo & Falstad (2013), weighing the contribution from each component, as well as including the effect of disc thickness (as explained in Chapter 2.2.2). This resulted in the Romeo-Falstad instability parameter for a multicomponent disc:

$$\frac{1}{Q_{RF}} = \sum_i \frac{W_i}{T_i Q_i}, \quad (2.6)$$

where W_i is the weight factor for component i (for example stars or gas) accordingly:

$$W_i = \frac{2\sigma_m \sigma_i}{\sigma_m^2 + \sigma_i^2} \quad (2.7)$$

m corresponds to the component that dominates the instability, i.e. $T_m Q_m = \min(T_i Q_i)$. T_i is the effect of disc thickness, as explained in Chapter 2.2.2, its value depending on the ratio of radial and vertical velocity dispersion, σ_z/σ_R , according to Eq. (2.4). In particular, for a two component disc the Romeo-Falstad instability parameter takes the following form:

$$\frac{1}{Q_{RF,2}} = \frac{W_{gas}}{T_{gas} Q_{gas}} + \frac{W_*}{T_* Q_*}. \quad (2.8)$$

The number of components needs to be determined and constrained. In a stability analysis it is first and foremost important to treat stars as a separate component

from gas. Thereafter we note that the interstellar gas mainly consist of hydrogen, where molecular hydrogen is believed to be the main ingredient in star formation. The neutral atomic hydrogen is abundant, easily detected and can have velocity dispersions comparable to that of the molecular gas, while the high velocity dispersions of ionised hydrogen makes it unlikely to greatly participate in gravitationally collapsing clouds. Consequently, a three-component analysis using stars, atomic hydrogen and molecular hydrogen can be found suitable ($i = \{stars, HI, H2\}$ in Eq. (2.6)).

2.2.6 The characteristic instability wavelength

As explained in Chapter 2.2.1 the stability analysis are subject to the condition of local axisymmetric perturbations, in other words: $kR \gg 1$, called the short-wavelength approximation. k is the least stable radial wavenumber, which be approximated as $k \sim \kappa/\sigma_m$ (Romeo & Falstad, 2013). From this k we can find the smallest scales of collapse as the characteristic instability wavelength:

$$\lambda = 2\pi \frac{\sigma_m}{\kappa}. \quad (2.9)$$

As can be seen in Fathi et al. (2015), Romeo & Fathi (2015) and Romeo & Fathi (2016) the characteristic instability wavelength can be utilised to detect hidden structures in a galaxy, e.g. bars within bars, nuclear starbursts and nuclear rings. The characteristic instability wavelength accurately predicts the radial locations and extent of starbursts, bars, CRs and other structures. Worth noting however, is that the feature in the graph indicating the structure can be due to either σ or κ , as can be understood from Eq. 2.9.

2.3 Observational background

An instability and structural study of a three-component galactic disc require data for each component. The HI data for this work is obtained from The HI Nearby Galaxy Survey (THINGS), for H2 the data is deduced from the HERA CO-Line Extragalactic Survey (HERACLES) as well as Berkley-Illinois-Maryland Association Survey of Nearby Galaxies (BIMA SONG). The surface density of stars are provided by Spitzer Infrared Nearby Galaxies Survey (SINGS).

THINGS is a spatial and spectral survey of the 21 cm line emission of 34 galaxies (Walter et al., 2008), and provides the surface density of HI. HERACLES maps the CO $2 \rightarrow 1$ line emission over the entire optical disc, and thereby deduces the surface density of H2 (Leroy et al., 2009), while BIMA SONG maps the CO $1 \rightarrow 0$ line instead and thereby obtains the H2 surface density (Helfer et al., 2003). HERACLES attains a higher sensitivity and are thereby more suitable for outer regions of galaxies, while BIMA SONG has a higher resolution which is more useful when observing inner regions. The surface density of stars are provided by SINGS, an infrared imaging and spectroscopic survey studying the infrared emission of 75 nearby galaxies, in an attempt to facilitate the connection between star formation and interstellar medium (Kennicutt et al., 2003).

Data from these four surveys have been compiled by Leroy et al. (2008) for a sample of the galaxies that are recurring in all the surveys. This results in a total of 11 dwarf galaxies and 12 spiral galaxies. In the study carried out in this thesis, only the spiral galaxies are considered.

2.3.1 Leroy et al. (2008): data and modelling

The model adopted by Leroy et al. (2008) include a number of assumptions in the treatment of the data. The velocity dispersion of gas and stars are the main issues, and there are assumptions and approximations to facilitate:

1. The velocity dispersions of HI and H2 are observationally motivated, approximated to constant values throughout the disc. Leroy et al. (2008) provide $\sigma_{HI} = 11\text{km/s}$, while Wilson et al. (2011) set $\sigma_{H2} = 6\text{km/s}$ ².
2. It is reasonably assumed that the disc is in vertical hydrostatic equilibrium, which means that the velocity dispersion perpendicular to the radial direction, $\sigma_{*,z}$, does not change with the scale height of the galaxy.
3. The scale height, on the other hand, is assumed to be constant with radius, which is generally not true, especially at large radii's (the interested reader can look up warping and flaring of discs).
4. To derive the scale height of the galaxy, only stars are considered as a factor.
5. The relation between the scale height of the disc and the radial scale length is deduced statistically, and is unfortunately subject to a notable amount of scatter.
6. Moreover the relation between the vertical and radial velocity dispersion is fixed at $\sigma_{*,z} = 0.6\sigma_{*,R}$. 0.6 may be reasonable for most-late type galaxies, but the value is believed to actually be a function of Hubble type.

Using the last five approximations, Leroy et al. (2008) deduce the velocity dispersion of the stars:

$$\sigma_* = \sigma_{*,R} = \frac{1}{0.6} \sqrt{\frac{2\pi G l_*}{7.3} \Sigma_*^{0.5}} \quad (2.10)$$

where l_* is the stellar scale length, which together with the stellar surface density Σ_* is provided in the paper by Leroy et al. (2008).

²It is worth noting that the velocity dispersion of the molecular gas, σ_{H2} , is a lower limit, and the velocity dispersion of atomic hydrogen can indicate the upper limit of σ_{H2} , i.e. $6 < \sigma_{H2} < 11\text{km/s}$.

3

Results & Discussion

This chapter depicts the results of the stability analysis of the 12 THINGS spirals, using both the multi-component Q stability parameter and the characteristic instability wavelength. Firstly, the galaxy sample as a whole is presented in Chapter 3.1. The difference between a classical Safronov-Toomre parameter for molecular gas and a Romeo-Falstad three-component Q stability parameter is shown, together with the characteristic instability wavelength for the one and three-component case. Thereafter, in Chapter 3.2, five galaxies have been chosen for a more extensive study. All the individual Toomre parameters and characteristic instability wavelengths are confronted, as well as the three-component cases for each parameter and galaxy. The five galaxies in Chapter 3.2 have been selected since there are reliable detections in literature of resonances and structures, such as bars and rings. The radial profiles for the five chosen galaxies: NGC 6946, NGC 3351, NGC 7331, NGC 3627 and NGC 628, are found in Chapter 3.2, while the radial profiles for the other 7 galaxies: NGC 2841, NGC 3184, NGC 3198, NGC 3198, NGC 4637, NGC 5055 and NGC 5194, are presented in Appendix B. The radial profiles of the galaxies are in several cases scaled with R_{25} , which is the optical radius of the galaxy¹. This chapter, Chapter 3, ends with a discussion focused on the importance of adequate radial profiles of the epicyclic frequency and velocity dispersions (Chapter 3.3).

3.1 The whole sample of THINGS spirals

The whole sample of THINGS spirals are the 12 spirals included in the paper by Leroy et al. (2008): NGC 628, NGC 2841, NGC 3184, NGC 3198, NGC 3351, NGC 3521, NGC 3627, NGC 4637, NGC 5055, NGC 5194, NGC 6946 and NGC 7331. The results of the study of the stability parameter and characteristic instability wavelength of these galaxies as a whole, are presented below.

3.1.1 The stability parameter

The left graph in Fig. 3.1 shows the classical Toomre parameter for molecular gas, Q_{H_2} . The scatter is rather large, while the three-component Q stability parameter of Romeo & Falstad (2013), Q_3 , seen to the right in Fig. 3.1, has a scatter contained within one order of magnitude. Note that the data points are colour-coded according

¹The optical radius was defined by Holmberg in 1958 as the radius of the major-axis corresponding to a surface brightness of 26.5 magnitude arcsec⁻² (https://ned.ipac.caltech.edu/level15/Faber/Faber3_1.html).

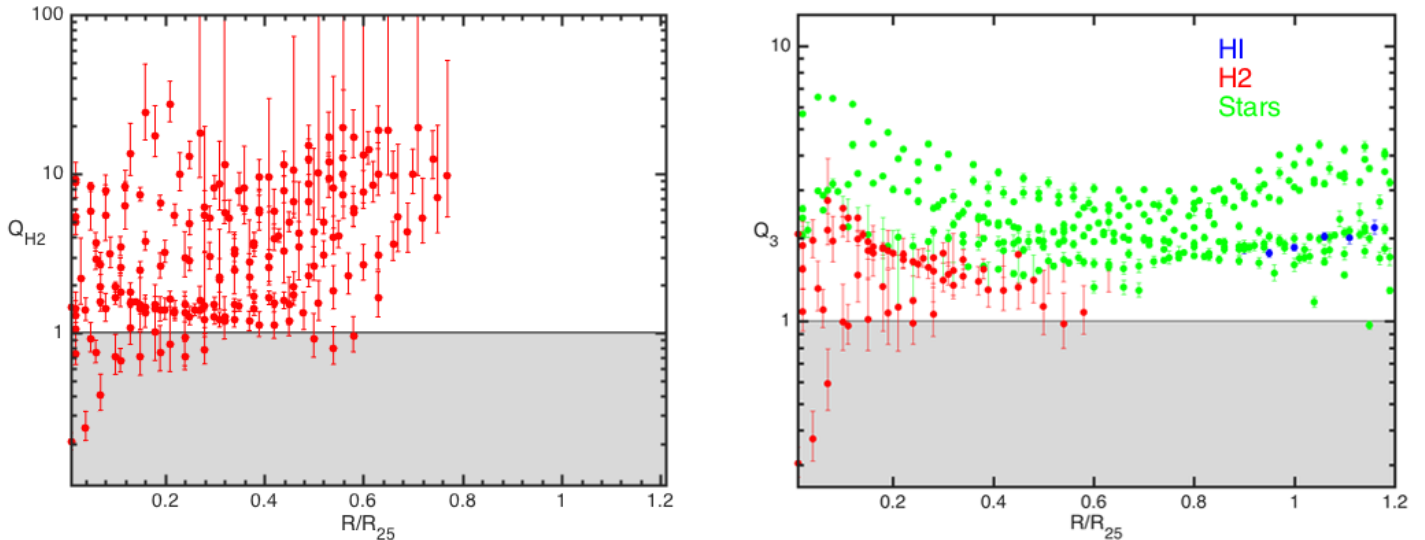


Figure 3.1: To the left: the classical Toomre parameter of molecular gas, Q_{H_2} , for the 12 spiral galaxies. To the right: the three-component stability parameter of Romeo & Falstad (2013), Q_3 , for the same set of galaxies. Notice the difference in maximum values of the y-axes. The data points are colour-coded indicating which component dominates the instability; HI-dominated points are blue, H2-dominated are red and star-dominated are green.

to which component dominates the instability. The large error bars of Q_{H_2} indicate the approach of the detection limit of the HERACLES survey.

One cause of the large scatter in Q_{H_2} (Fig. 3.1 left), compared to the Q_3 , is the effect of heating (gravitational instabilities that give rise to a higher velocity dispersion) and cooling (by dissipation which decrease the value of the Q stability parameter again), further discussion is found in Romeo & Falstad (2013). The total three-component Q parameter is not largely affected by these fluctuations due to self-regulation in the galactic disc, which is reflected by the weight factors, W_i in Eq. (2.6). This means that Q_3 is the more suitable control parameter for the instability of galactic discs.

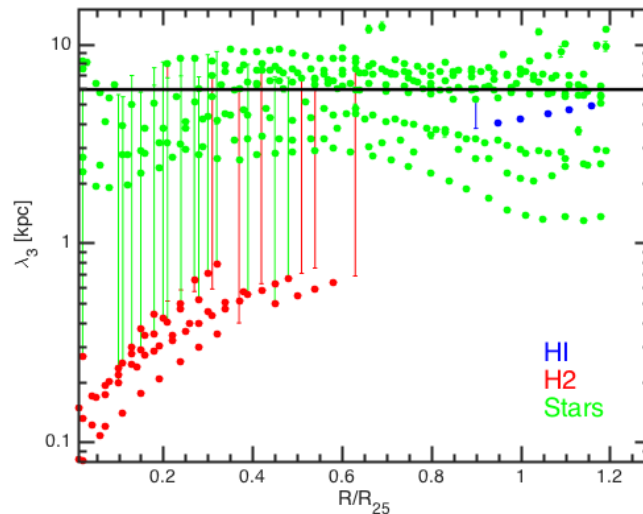


Figure 3.2: The characteristic instability wavelength for a three-component disc: stars, HI and H2. The horizontal black line shows the median value of the characteristic instability wavelength for the stars of ≈ 6 kpc.

3.1.2 The characteristic instability wavelength

The characteristic instability wavelength for the three-component disc, λ_3 , is displayed in Fig. 3.2. Generally the galaxies either have an instability dominated by stars or by molecular gas, well separated in the graph. Molecular gas dominate only in the inner regions, up to an optical radius of about $0.6R_{25}$. Molecular gas dominate the instability on λ_3 scales of only a few 100 pc, while the stars dominate on scales of a few kpc. Notice that HI domination is present only at the edge of the optical disc, and only for NGC 3198 (individual radial profile can be seen in Fig. B.3). The star-dominated characteristic instability wavelength varies less than one order of magnitude, with a median value for the whole sample of spirals and for all radii of 6 kpc, and a 1σ scatter of 2.5. Studying the galaxies individually suggests that a galaxy of a smaller size is related to a lower median value for the star-dominated λ_3 .

Fig. 3.3 illustrates the characteristic instability wavelength for molecular gas alone, λ_{H2} . Note that the data points are distributed in two bands with a gap in between. The gap is most likely due to a lack of spread in the sizes of galaxies, since the slope of λ_{H2} with the steepest rise corresponds to the galaxy with the largest optical radius, R_{25} , and the smaller the galaxy's optical radius is the flatter is the λ_{H2} .

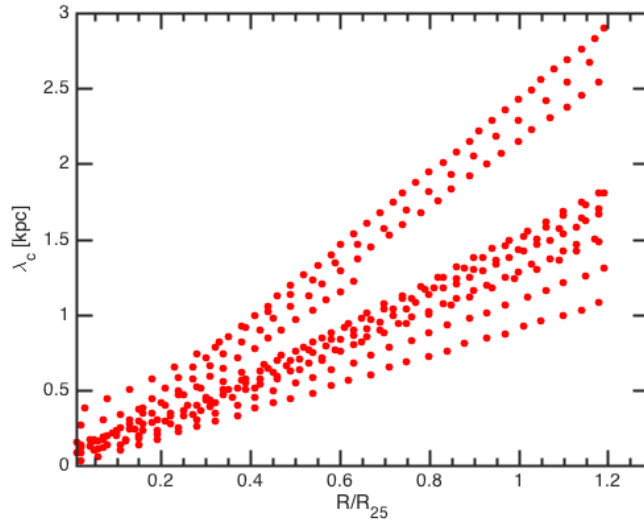


Figure 3.3: The characteristic instability wavelength for molecular gas.

3.1.3 Correlation with the mass distribution

In Fig. 3.3 we can see a linear relation between λ_{H_2} and the radius of the galaxy, scaled with the optical radius, R_{25} . Since the velocity dispersion of H₂ is assumed constant (as stated in Chapter 2.3.1) the characteristic instability wavelength for molecular gas is inversely proportional to the epicyclic frequency, as seen in Eq. (2.9): $\lambda_{H_2} \propto 1/\kappa$. The epicyclic frequency, on the other hand, is deduced from the rotation curve. Since the distribution of mass is expected to affect the rotation curve, we would like to check the correlation of total mass of the galaxy and slope of λ_{H_2} . The total mass, M , of the galaxy, is the mass within the optical radius, R_{25} , and can be estimated as:

$$M = \frac{v_{flat}^2 R_{25}}{G} \quad (3.1)$$

where v_{flat} is the velocity of the flat part of the rotation curve, provided by Leroy et al. (2008). Fig. 3.4 show the slope of λ_{H_2} as a function of the total mass of the galaxy, and there is no clear correlation visible. If we instead look at the compactness of the galaxy, that is the volume and surface density of the galaxy, perhaps a correlation can be found. The relation of total mass of a galaxy to average volume density, $\langle \rho \rangle$, as well as to average surface density, $\langle \Sigma \rangle$, is:

$$\langle \rho \rangle = \frac{M}{\frac{4\pi}{3} R_{25}^3} \quad (3.2)$$

$$\langle \Sigma \rangle = \frac{M}{\pi R_{25}^2}. \quad (3.3)$$

In Fig. 3.5, the correlation between the slope of λ_{H_2} and the two compactness parameters, $\langle \rho \rangle$ and $\langle \Sigma \rangle$, is displayed. The average volume density correlates the strongest to the slope of λ_{H_2} , while the correlation is weaker for the surface density. So it is the compactness of the galaxy, and not the mass itself, that is connected to the slope of λ_{H_2} .

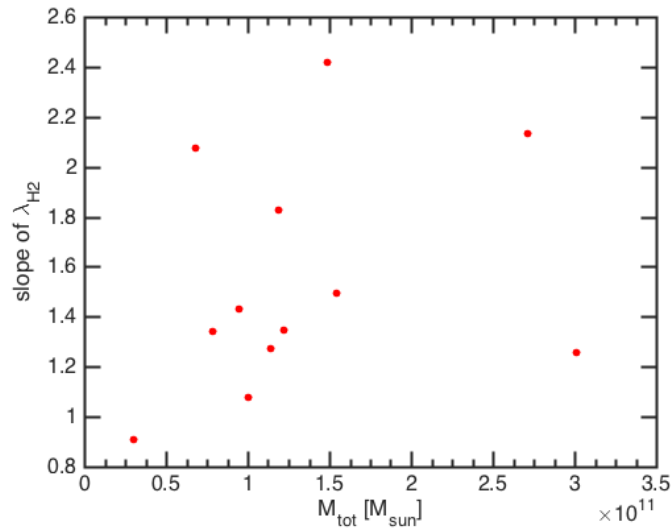


Figure 3.4: A look into the correlation of total galaxy mass and the slope of λ_{H2} . The x-axis states the total mass of the galaxy, and the y-axis the slope of λ_{H2} .

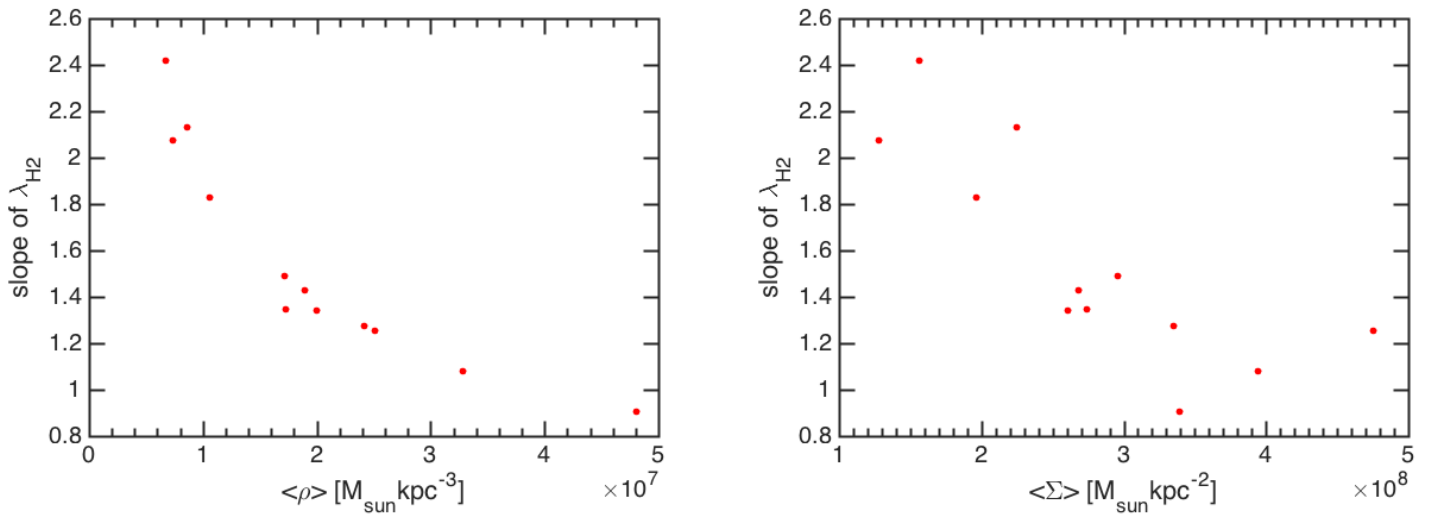


Figure 3.5: The correlations between the slope of λ_{H2} and the compactness of the galaxy. To the left the average volume density of the galaxy is plotted against the slope of λ_{H2} , while to the right it is the average surface density against the slope of λ_{H2} .

3.2 Is there a relation between the characteristic instability wavelength and local structures in galactic discs?

The galaxies chosen for analysis using the characteristic instability wavelength are, in order of importance regarding interesting features: NGC 6946, NGC 3351, NGC 7331, NGC 3627 and NGC 628. Since these are nearby galaxies, the conversion from arcseconds (") to actual sizes can be approximated using:

$$\text{size[pc]} \sim 4.85 \cdot \text{angular size[arcsec]} \cdot \text{distance[Mpc]}$$

The positions of resonances and structures in the following chapters are approximate locations, the original literary sources do not always provide uncertainties, and the uncertainty and radial extent of the structure can be large.

3.2.1 A case study: NGC 6946

NGC 6946 is a SAB(rs)cd galaxy located at a distance of 5.9 Mpc². Romeo & Fathi (2015) provide satisfactory information, their data is based on the same inclination and position angle as adopted by Leroy et al. (2008). Romeo & Fathi (2015) locate a large weak bar with a radial extent of 270"; a secondary bar (SB) of 60"; a nuclear bar (NB) of 8"; and a nuclear star forming region (NS) at 5.5". The corotation of the weak bar-like structure is located at 250 – 300", the oILR at 30 – 60" and the iILR at 15". Tamburro et al. (2008) provide the corotation radius of the pattern: $CR_T = 176''$. They use: $i = 32.6^\circ$ and P.A. = 242° , compared to the values of Leroy et al. (2008) of $i = 33^\circ$ and P.A. = 243° .

The stability analysis of Romeo & Fathi (2015) provide the graphs seen in Fig. 3.6. In the graph to the left, the stability parameter of molecular gas, Q_{H_2} , provides vague indications of the presence of the nuclear starburst and the secondary bar. On the other hand, the graph to the right in Fig. 3.6, depicts the characteristic instability wavelength for the molecular gas, and two structural features are clearly indicated by two well separated minima in the curve. It can thereby be seen that the Q parameter is a much noisier diagnostic than the characteristic instability wavelength, and that λ is a powerful diagnostic for accurately predicting the sizes of the local structures (such as starbursts and bars) in the disc. The thick blue lines in Fig. 3.6 are the fits of the respective parameters.

Using the coarser resolution of the data of Leroy et al. (2008) for the entire radial range available results in the graphs of Fig. 3.7. Studying the top graphs in Fig. 3.7 reveals the SB located exactly at the first maximum in Q , right after the unstable inner region of the galaxy. The outer ring (large weak bar) is located where there is no longer any detection of molecular gas, which also coincides with the CR of the bar.

²All distances to galaxies in this thesis are acquired from Leroy et al. (2008).

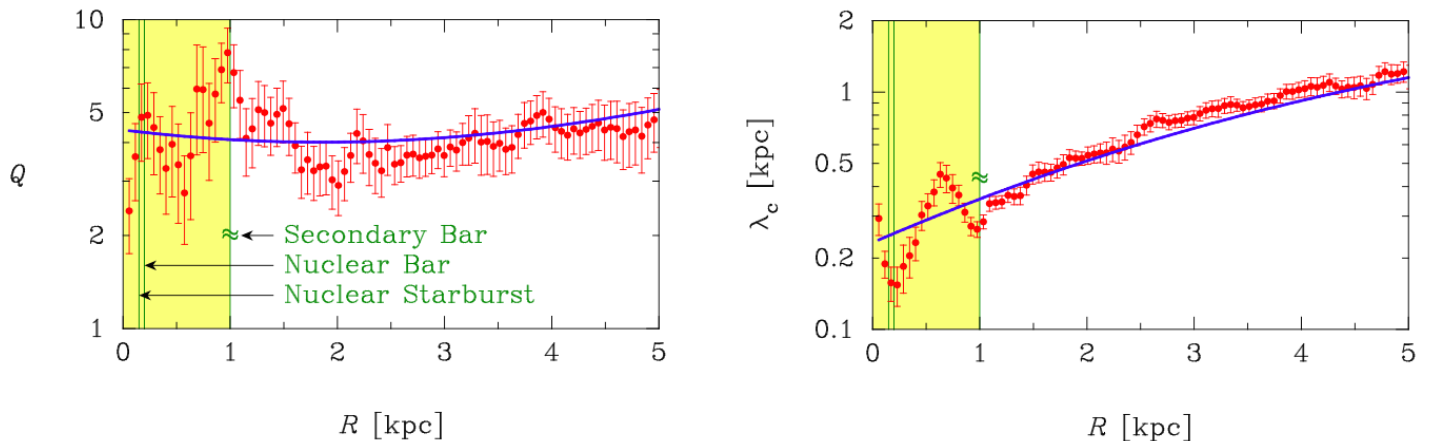


Figure 3.6: The left graph illustrates the Q stability parameter for the molecular gas in NGC 6946, while the right contains the characteristic instability wavelength for the same, from Romeo & Fathi (2015). The thick blue lines are the fits of the respective parameters, and the vertical lines represent the radial extents of (from left to right): NS, NB and SB.

The smoothed out epicyclic frequency and assumed constant velocity dispersions³ of Leroy et al. (2008) has a clear effect on the curve. The region in Fig. 3.6 (right graph), that showed the two minima for the NS and SB, are completely smoothed out and the curve in Fig. 3.7 (bottom right) is just the approximation of the one in Fig. 3.6. On the other hand the CR_T in the graph in the bottom left of Fig. 3.7 clearly indicate the sharp change from a stability parameter dominated by molecular gas to a stability parameter dominated by stars, something the Q stability parameter is unable to do.

3.2.2 NGC 3351

Swartz et al. (2006) provide us with the radius of the bar, $47''$, in this SB(r)b galaxy. The bar is surrounded by a ring at a radial distance of $47 - 67''$, and there is also a circumnuclear region, CNR, at $5.10'' - 7.14''$. Tamburro et al. (2008) provide the corotation radius of the pattern as $119''$, using the same inclination angle as Leroy et al. (2008). The distance adopted to this galaxy is 10.1 Mpc. Devereux et al. (1992) position the bar at $59''$, the ring at $66''$ and the CNR at $7''$, similar to the results by Swartz et al. (2006). Devereux et al. (1992) also find a small nuclear bar at a size smaller than $19''$, aligned perpendicular to the large scale stellar bar. The inclination that Devereux et al. (1992) have adopted is one degree larger than the value used by Leroy et al. (2008). The large discrepancy is in the major axis position angle, Devereux et al. (1992) have chosen 13° while Leroy et al. (2008) have 192° . Swartz et al. (2006) made the choice of position angle of 15° , but using the same inclination as Leroy et al. (2008). Combining the values of these three papers should

³Romeo & Fathi (2015) adopt an observationally deduced velocity dispersion for H₂ with a median of 10km/s, in comparison to the 6km/s used in the analysis in this thesis. This is the cause of the slight difference in y-axis values between the two curves in the graphs (Fig. 3.6 and Fig. 3.7).

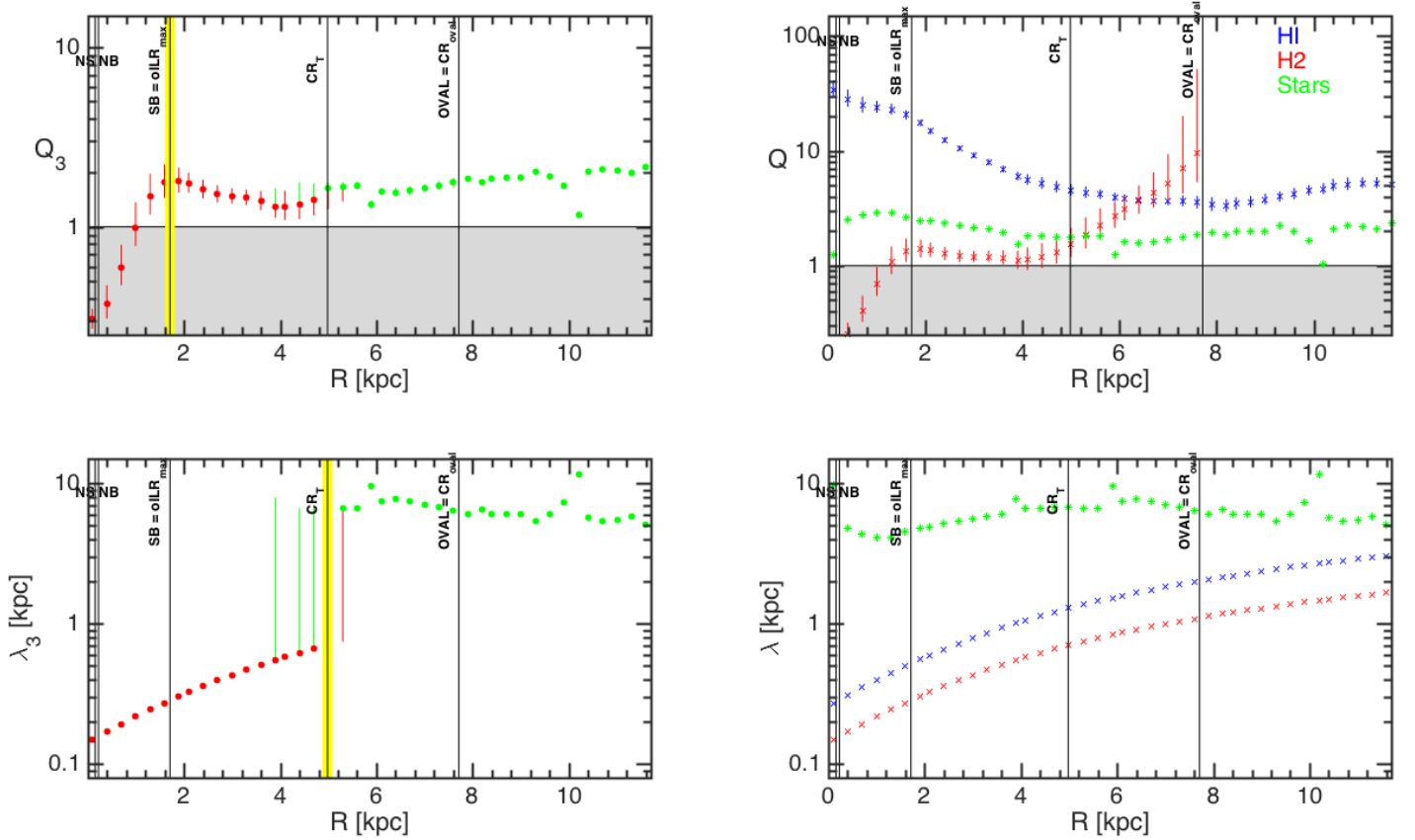


Figure 3.7: Radial profiles for NGC 6946 (SAB(rs)cd); The three-component Romeo-Falstad Q stability parameter (top left), the classical Safronov-Toomre parameter for each component (top right), the three-component characteristic instability wavelength (bottom left) and the characteristic instability wavelength for the individual components (bottom right). The vertical lines indicate the radial extents of the structural features in NGC 6946. The vertical lines are labelled, from left to right, as: NS, NB, SB = oILR_{max}, CR_T, OVAL \approx CR_{oval}.

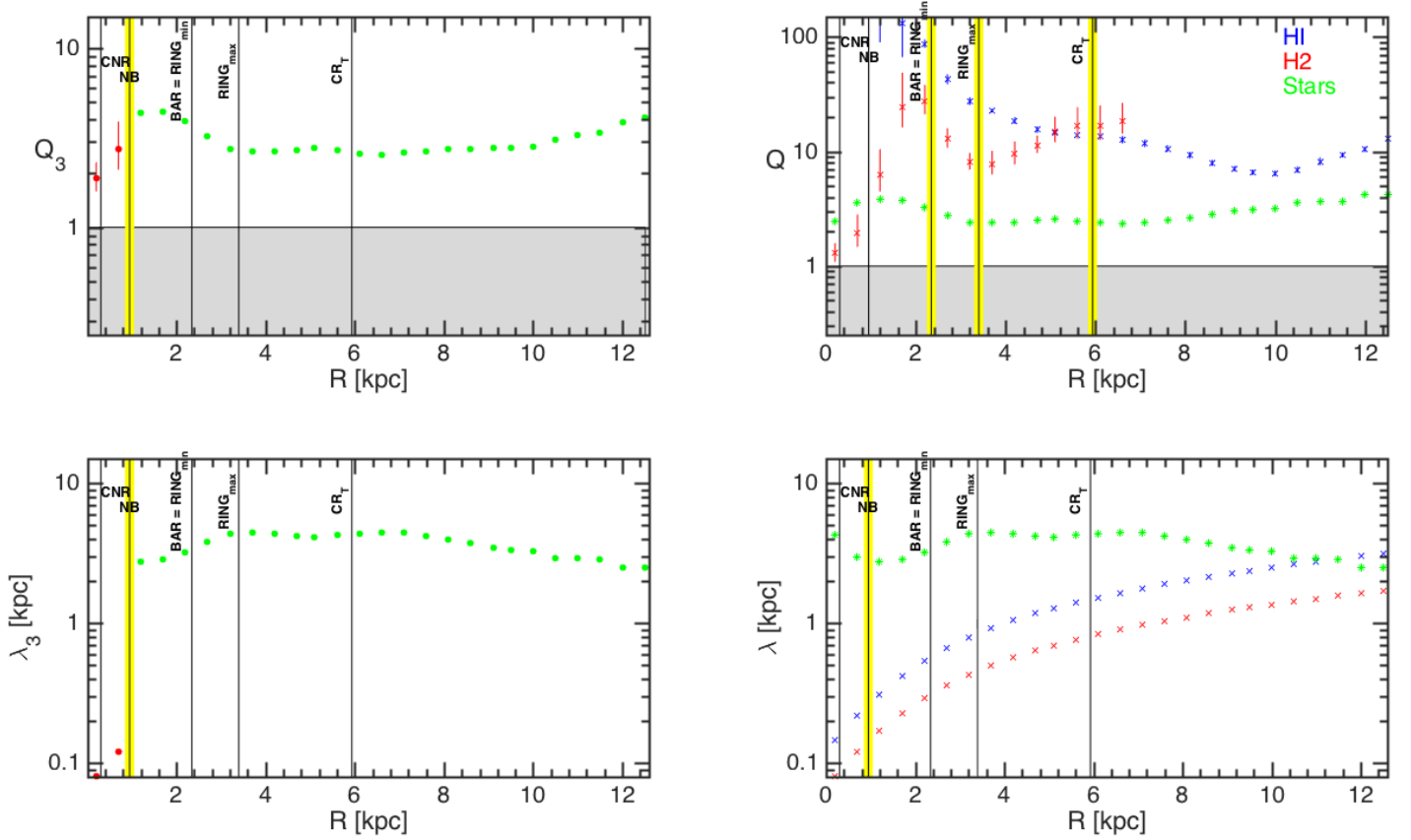


Figure 3.8: Same as Fig. 3.7 but for NGC 3351 (SB(r)b). The vertical lines are labelled, from left to right, as: CNR (6.1"), NB (19"), BAR = RING_{min} (47"), RING_{max} (67"), CR_T (119"). Where the values chosen for the vertical lines are added within the parentheses, since there are several mentioned in the text.

therefore be done with slight caution, due to this large discrepancy in position angle.

In the top right of Fig. 3.8 the Q stability plot show the maximum of the radial extent of the ring (ring_{max}) located at a lower Q_{H2} value than the surroundings, while the bar/ring_{min} and CR_T is related to separate Q_{H2} maxima. Located close to the maximum in the Q_3 is the nuclear bar (NB), which also coinciding with the shift of the component that dominates the instability, from stars to H2. This transition is clearly visible by the discontinuity in λ_3 , in the bottom left graph of Fig. 3.8. In the bottom right graph in this figure, we can also see that the NB is related to a minimum in the characteristic instability wavelength for the stars.

3.2.3 NGC 7331

Mediavilla et al. (1997) describe this SA(s)bc galaxy as a galaxy with a counter-rotating stellar bulge. They locate a CNR in the inner $12'' \times 9''$ and a ring of ionised gas at a radius of $38''$. The inclination and position angle is set to $i = 75^\circ$ and P.A= 170° , compared to Leroy et al. (2008): $i = 76^\circ$ and P.A= 168° . von Linden et al. (1996) on the other hand use $i = 75^\circ$ and P.A= 165° . NGC 7331 is located at a distance of 14.7 Mpc. The CO observations of von Linden et al. (1996) do not prove directly the presence of a nuclear bar, however the dynamics of the inner disc hint at the presence of a small evolved bar depleted from molecular gas, with a radial size of $15''$. The CO observations show an extended torus-like accumulation of molecular gas at a galactocentric radius of $44'' - 74''$. This molecular gas torus is most probably located at the ILR and extends to the CR at $74''$.

In Fig. 3.9 the two top graphs show the three-component stability parameter and the individual Safronov-Toomre parameters. The CR together with the maximum radial extent of the ring mark a transition between the two different components dominating the instability: molecular gas and stars. The NB is located at the maximum of the three-component stability parameter, Q_3 , close to the centre of the galaxy. The characteristic instability wavelength for NGC 7331 show two distinct transitions between the two components that dominate the instability (see Fig. 3.9). The rightmost one is pinpointed by the CR/ring_{max}, while the left transition from star to H₂ domination cannot be related to any structural feature. However, this inner region of NGC 7331 is in violation of the short-wavelength approximation, see Appendix A and the discussion below in Chapter 3.3.

3.2.4 NGC 3627

NGC 3627 is a two-armed barred SAB(s)b galaxy, at a distance of 9.3 Mpc. Tamburro et al. (2008) show no discrepancy with Leroy et al. (2008) concerning inclination and position angle, and provide the corotation radius as $160''$. Rand & Wallin (2004) use BIMA SONG data and discover an indication in the HI observations of a tidal encounter with the galaxy NGC 3628. The CO map together with near-IR images indicates a bar of $48''$, and a weak ring at $68''$. The CR for the bar is assumed to 1-1.4 bar radii, i.e $49'' - 69''$, located between the bar and the ring. Rand & Wallin (2004) adopt $i = 65^\circ$ and P.A= $170 \pm 5^\circ$, similar to Leroy et al. (2008) ($i = 62^\circ$ and P.A= 173°).

The top left graph in Fig. 3.10 hint that the ring can be associated with a minimum of Q_3 at $R \approx 3\text{kpc}$, perhaps in an attempt to facilitate star formation. In the two bottom graphs in Fig. 3.10, the characteristic instability wavelength shows us a wide transitional region between the two components that dominate the instability.

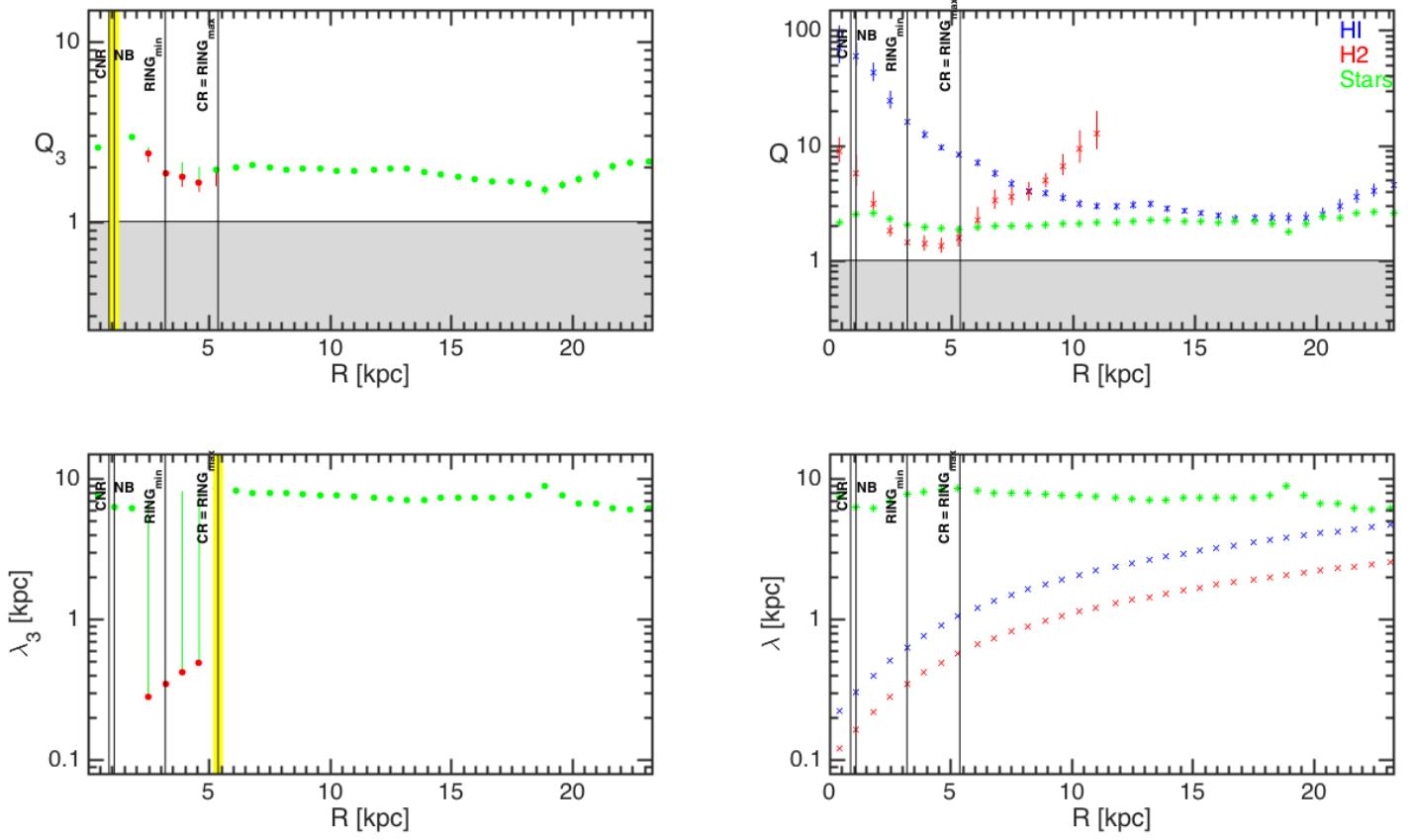


Figure 3.9: Same as Fig. 3.7 but for NGC 7331 (SA(s)bc). The vertical lines are labelled, from left to right, as: CNR, NB, $RING_{min}$, $CR = RING_{max}$.

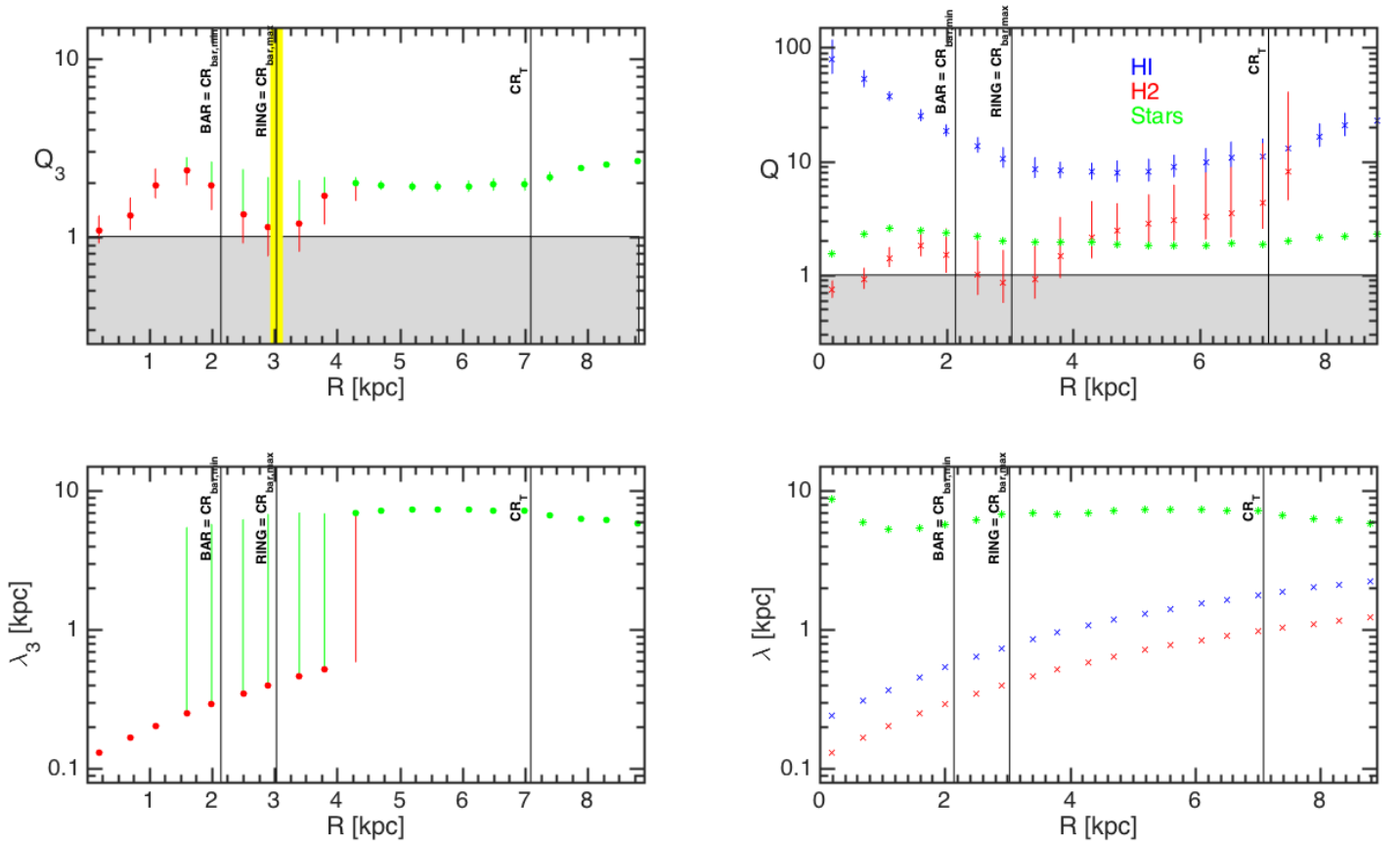


Figure 3.10: Same as Fig. 3.7 but for NGC 3627 (SAB(s)b). The vertical lines are labelled, from left to right, as: BAR = $CR_{bar,min}$, RING = $CR_{bar,max}$, CR_T .

3.2.5 NGC 628

NGC 628 is a non-interacting SA(s)c galaxy, located at a distance of 7.3 Mpc. Fathi et al. (2007) describe a galaxy with a weak bar of radial length $2''$ in the centre. A nuclear ring is located at the ILR of the pattern at just below $1 \text{ kpc} \approx 19''$ and an oval at $42''$. The CR is positioned at a radial distance of $110''$. Tamburro et al. (2008) have also studied the CR of the large scale pattern in NGC 628, and located it at $145''$. Fathi et al. (2007) adopt values of the inclination and position angle of the galaxy, which only slightly deviate from the values adopted by Leroy et al. (2008). Fathi et al. (2007) use: $i = 6.5^\circ$ and $P.A. = 25^\circ$, compared to the values of Leroy et al. (2008) of $i = 7^\circ$ and $P.A. = 20^\circ$. This is a well studied galaxy, but the results are subject to discrepancies, which is especially clear in the paper by Zhang & Buta (2015). Zhang & Buta (2015) have used a different method than Fathi et al. (2007) and Tamburro et al. (2008), and thereby found five different corotation resonances in this galaxy. The reason for so many CRs is explained to be caused by the many different pattern speeds in this young galaxy, a galaxy that has not yet

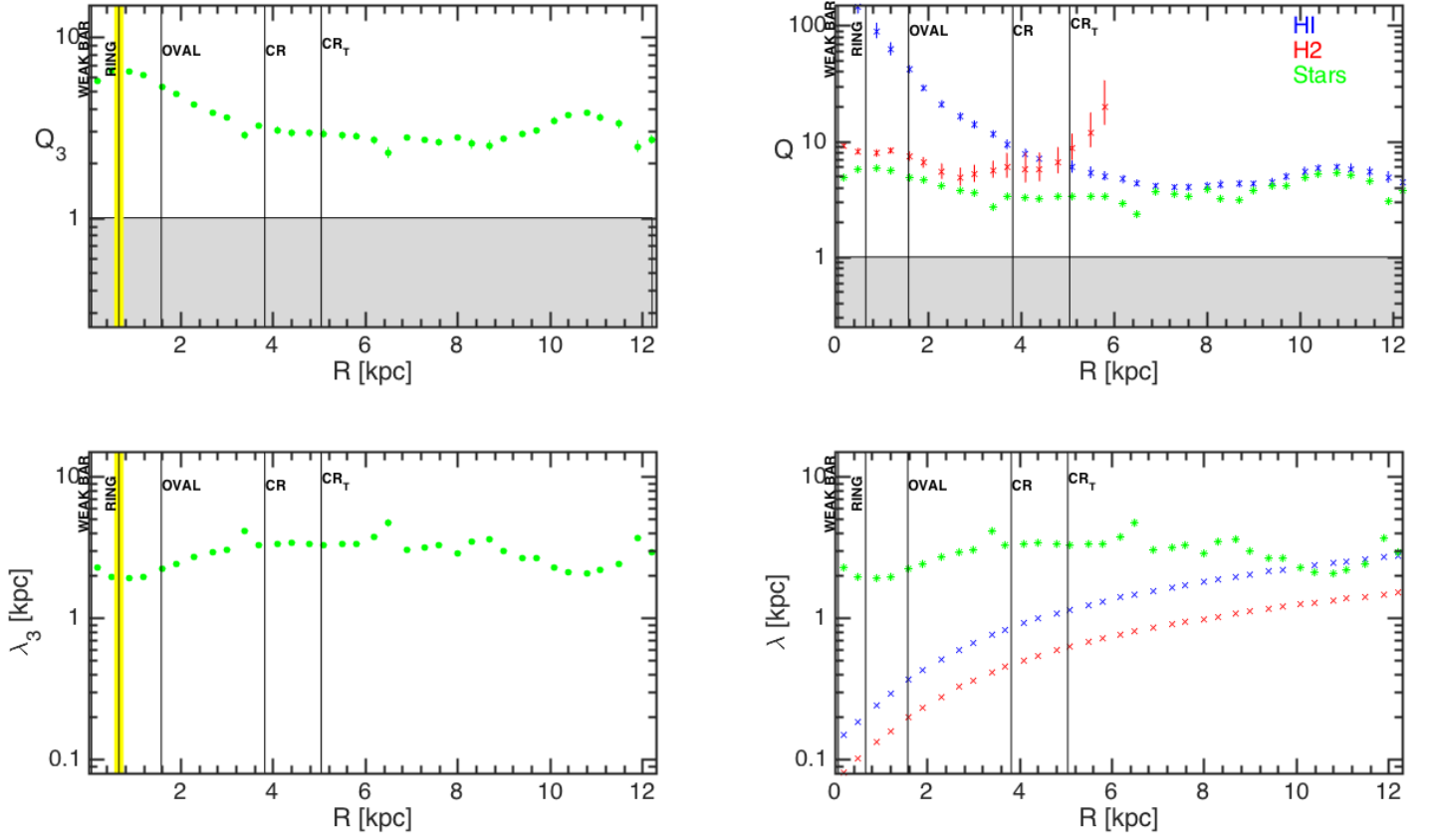


Figure 3.11: Same as Fig. 3.7 but for NGC 628 (SA(s)c). The vertical lines are labelled, from left to right, as: WEAK BAR, RING, OVAL, CR (the CR of Fathi et al. (2007)), CR_T (the CR of Tamburro et al. (2008)).

settled down into a common rotational speed. But this method requires more work and better resolution in simulations before it will be able to reach its full potential.

The leftmost graphs in Fig. 3.11 hint at a relation between the location of the ring with a maximum of Q_3 , as well as a minimum of λ_3 . Worth noting is that the bump in Q_3 is only related to the stability parameter for the stars, as the bump is not occurring in the stability parameter for the HI or H2 (see the top right graph in Fig. 3.11). A slight dip in Q_{H2} is hinted upon instead. For the characteristic instability wavelength, it is only the star dominated data that indicate the minimum since the characteristic instability wavelengths for the gas is too smoothed out.

3.2.6 Any other features?

The most striking is the new ability of the characteristic instability wavelength. The characteristic instability wavelength provides a sharp and distinct indication when the component that dominates the instability changes. This transition often coincides with a structural feature as well, see for example the CR_T in NGC 6946, Fig. 3.7.

In the inner region of the galaxies there is a dip in the characteristic instability wavelength for the stars (see for example Fig. 3.8 where this dip is surrounded by the CNR and the ring). The structural features hint at favouring locations surrounding this dip:

- small weak bars, NB, NS and CNR : the left slope
- Bar/SB : rightmost slope
- Ring : the top right (except for in the only galaxy with an oval: NGC 628, where the ring is located between the weak bar and the oval)

3.3 Discussion

In this chapter the focus is on the importance of the velocity dispersion and epicyclic frequency, concerning the application of the characteristic instability wavelength as a diagnostic to spiral galaxies. The chapter also includes details on the latest movements in velocity dispersion determination. But first of all, it is worth noting how reassuring it is that almost all the data points for all THINGS spirals satisfies the short-wavelength approximation ($\lambda \ll 2\pi R$), see Appendix A.

However, it is very complicated to deduce reliable information about hidden structures, such as bars within bars, nuclear rings and resonances in galaxies. The most common method of choice today is the method of Tremaine & Weinberg (1984). This method is unfortunately difficult to apply and even within the same galaxy the results can diverge, see for example NGC 5055 in Appendix B, Fig. B.6, where the location of the CR of the spiral pattern is set to 120-180" by one source and to 260" by another, resulting in a range of approximately 7 kpc. The new diagnostic of the characteristic instability wavelength deduced from radial profiles of the velocity dispersion and epicyclic frequency, does show great promise. When a constant value of the velocity dispersion of gas is assumed the value chosen is rather important, which can be seen through a comparison with Romeo & Fathi (2015). Romeo & Fathi (2015) provide a median value of the velocity dispersion of molecular gas of 10 km/s for NGC 6946, compared to the value of 6 km/s adopted in the analyses carried out in this thesis. If the value of Romeo & Fathi (2015) is applied instead, the Q stability parameter and characteristic instability wavelength change, see Fig. 3.12. Studying the characteristic instability wavelength in Fig. 3.12 and Fig. 3.7, show that the hidden structure related to the sharp transition between the components that dominate the instability changes from the CR to the SB.

Romeo & Fathi (2015) began to reveal the power of the characteristic instability wavelength, using NGC 6946, as described in Chapter 3.2.1. Using radial profiles of adequate resolution for the velocity dispersion and epicyclic frequency of molecular gas, hidden structures (the secondary bar and the nuclear bar) of NGC 6946 was pinpointed. In Fig. 3.6 and Fig. 3.7, we can see that if a global model such as the model of Leroy et al. (2008) is adopted, a featureless radial profile of the characteristic instability wavelength is found (see the thick blue line in Fig. 3.6), and the hidden structures remain hidden. Thereby the importance of including the actual radial profiles is clear. For NGC 6946 the indications of the hidden structures show up in the radial profile for the epicyclic frequency alone, while in Romeo & Fathi (2016), where a characteristic instability wavelength analysis has been done of NGC 1068, the velocity dispersion is the parameter which contains the features of the structures. Thereby, we can see that radial profiles of adequate resolution for both the epicyclic frequency and the velocity dispersion are required to properly deduce the radial extent of the hidden structures.

3.3.1 Progress in the field

There are some progress done in this context, however the results do not yet converge. Based on the THINGS and the HERACLES survey, Caldú-Primo et al.

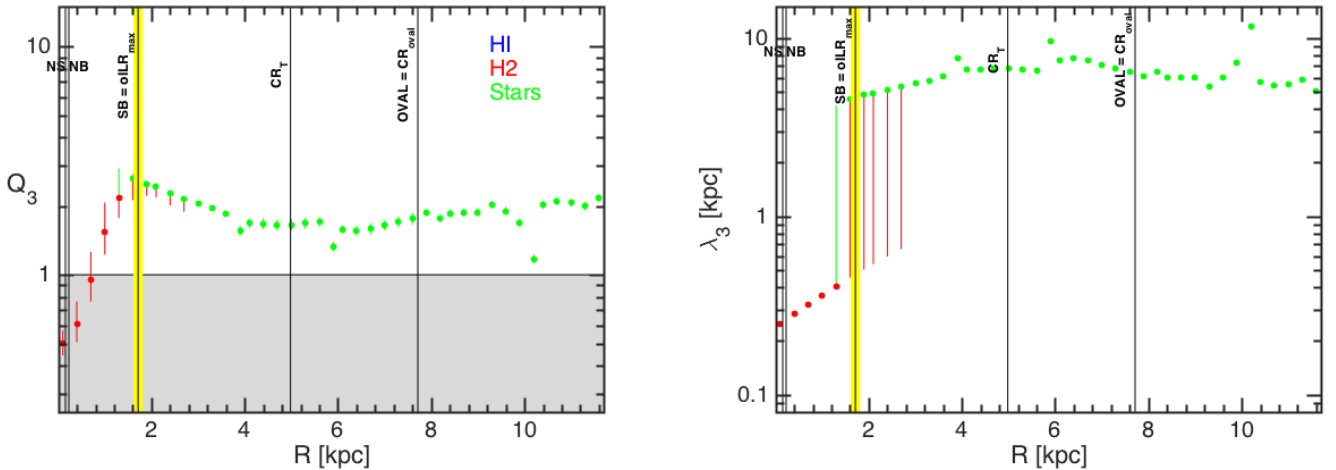


Figure 3.12: Radial profiles for NGC 6946 (SAB(rs)cd), using a constant velocity dispersion of 10km/s as deduced by Romeo & Fathi (2015); The three-component Romeo-Falstad Q stability parameter (left) and the three-component characteristic instability wavelength (right). The vertical lines indicate the radial extents of the structural features in NGC 6946. The vertical lines are labelled, from left to right, as: NS, NB, SB = oILR_{max}, CR_T, OVAL \approx CR_{oval}.

(2013) and Mogotsi et al. (2016) have attempted to model the velocity dispersion of atomic and molecular gas, while Ianjamasimanana et al. (2015) have worked on the velocity dispersion of atomic gas only. Generally they find velocity dispersions of $\approx 6 - 12\text{km/s}$, that increase towards the central regions of galaxies. Without considering the discrepancies between the results of Ianjamasimanana et al. (2015), Caldú-Primo et al. (2013) and Mogotsi et al. (2016), their radial profiles of velocity dispersions cannot yet be included in an analysis, such as the one carried out in this thesis. First of all, the radial profiles of the velocity dispersions are not publicly available, and secondly, radial profiles of surface densities are required as well.

However, as seen in Romeo & Fathi (2015) for NGC 6946, radial profiles of the epicyclic frequency are desired as well, and to deduce the epicyclic frequency adequate data of the rotation curve of the galaxy is required. de Blok et al. (2008) present rotation curves for the whole sample of THINGS spirals. This data would possibly improve the model adopted by Leroy et al. (2008) in the inner regions of the galaxies, where there is a steep increase in angular velocity close to the centre, which have not been adjusted for by Leroy et al. (2008). But despite any possible improvement of the model in the inner regions of galaxies, the resolution of the THINGS data is, as shown in Chapter 3.2.1, still too low to discern the smaller structural features such as bars within bars. As explained, the importance of a well resolved epicyclic frequency is evident in Romeo & Fathi (2015), while the weight of a radially dependent velocity dispersion can be seen in Romeo & Fathi (2016). Conclusively, this leaves us with the requirement of more extensive observations using higher resolution.

4

Conclusions

In this thesis, an exploratory study of the characteristic instability wavelength of 12 nearby spiral galaxies has been done, including a Q stability analysis thereof. The sample used is a well-analysed high-quality sample with data composed of four different surveys: The HI Nearby Galaxy Survey (THINGS), the HERA CO-Line Extragalactic Survey (HERACLES), the Berkley-Illinois-Maryland Association Survey of Nearby Galaxies (BIMA SONG), and the Spitzer Infrared Nearby Galaxies Survey (SINGS). The stability analysis carried out here provides the following insights:

- The characteristic instability wavelength can determine the radial extent of "hidden" structures (such as bars within bars, nuclear rings etc.), and is a less noisy diagnostic than the Q stability parameter of Romeo & Falstad (2013). On the other hand, the three-component Q stability parameter can be used for determining at which radii's a galaxy is gravitationally unstable, and which component (stars, atomic hydrogen or molecular hydrogen) that dominates the onset of instability. Both diagnostics are useful when performing a thorough analysis of the galaxy.
- Most interestingly, we have found that the characteristic instability wavelength has yet another power. Besides determining the locations of hidden structures, this parameter also has the ability to predict the transition between the components dominating the instability of the galaxy.
- The data provided by Leroy et al. (2008) can be used to study the radial profile of the characteristic instability wavelength in nearby star-forming galaxies. However, the resolution of such data is too low to discern the whole variety of structures hidden in the inner galaxy regions, such as nuclear rings, bars within bars etc. Observational data with higher resolution are required to reveal such hidden structures, and to continue to explore the potential of the characteristic instability wavelength.

The next step of this analysis would be to include observational radial profiles of gas and stellar velocity dispersions (see Chapter 3.3), so as to relax the strongest assumptions made by Leroy et al. (2008): the assumption of constant gas velocity dispersion and a model-based, rather than observational stellar velocity dispersion. My personal preference would be to focus on NGC 3351. NGC 3351 (see Chapter 3.2.2) shows a clear transition between the two components that dominate the instability (stars and molecular gas), marked by a nuclear bar. Will observational data of higher resolution provide a similar revelation as it did for NGC 6946 in Romeo

4. Conclusions

& Fathi (2015)? Will better data for NGC 3351 enable us to pinpoint the locations and extent of the circumnuclear region, the secondary bar and the ring as well? In addition for NGC 3351, Fig. 3.8 shows distinct features in the radial profile of the Q stability parameter for molecular gas. Are these features particular for NGC 3351 or more general for nearby star-forming spirals?

References

- Bertin, G. & Romeo, A. B. 1988, *A&A*, 195, 105
- Binney, J. & Tremaine, S. 2008, *Galactic Dynamics: Second Edition* (Princeton University Press)
- Caldú-Primo, A., Schrubba, A., Walter, F., et al. 2013, *AJ*, 146, 150
- Corradi, R. L. M., Boulesteix, J., Bosma, A., Amram, P., & Capaccioli, M. 1991, *A&A*, 244, 27
- de Blok, W. J. G., Walter, F., Brinks, E., et al. 2008, *AJ*, 136, 2648
- Devereux, N. A., Kenney, J. D., & Young, J. S. 1992, *AJ*, 103, 784
- Elmegreen, B. G. 1995, *MNRAS*, 275, 944
- Fathi, K., Beckman, J. E., Zurita, A., et al. 2007, *A&A*, 466, 905
- Fathi, K., Izumi, T., Romeo, A. B., et al. 2015, *Astrophysical Journal Letters*, 806, L34
- Helfer, T. T., Thornley, M. D., Regan, M. W., et al. 2003, *ApJS*, 145, 259
- Ianjamasimanana, R., de Blok, W. J. G., Walter, F., et al. 2015, *AJ*, 150, 47
- Jog, C. J. 1996, *MNRAS*, 278, 209
- Jog, C. J. & Solomon, P. M. 1984a, *ApJ*, 276, 127
- Jog, C. J. & Solomon, P. M. 1984b, *ApJ*, 276, 114
- Kennicutt, Jr., R. C., Armus, L., Bendo, G., et al. 2003, *PASP*, 115, 928
- Kormendy, J. 2013, *Secular Evolution in Disk Galaxies*, ed. J. Falcón-Barroso & J. H. Knapen, 1
- Kormendy, J. & Kennicutt, Jr., R. C. 2004, *Annual Review of Astronomy and Astrophysics*, 42, 603
- Leroy, A. K., Walter, F., Bigiel, F., et al. 2009, *AJ*, 137, 4670
- Leroy, A. K., Walter, F., Brinks, E., et al. 2008, *AJ*, 136, 2782

References

- Lin, C. C. & Shu, F. H. 1966, *Proceedings of the National Academy of Science*, 55, 229
- Mediavilla, E., Arribas, S., García-Lorenzo, B., & del Burgo, C. 1997, *ApJ*, 488, 682
- Meidt, S. E., Rand, R. J., Merrifield, M. R., Shetty, R., & Vogel, S. 2011, *Memorie della Societa Astronomica Italiana Supplementi*, 18, 133
- Mogotsi, K. M., de Blok, W. J. G., Caldú-Primo, A., et al. 2016, *AJ*, 151, 15
- Rafikov, R. R. 2001, *MNRAS*, 323, 445
- Rand, R. J. & Wallin, J. F. 2004, *ApJ*, 614, 142
- Romeo, A. B. & Falstad, N. 2013, *MNRAS*, 433, 1389
- Romeo, A. B. & Fathi, K. 2015, *MNRAS*, 451, 3107
- Romeo, A. B. & Fathi, K. 2016, *ArXiv e-prints* [[arXiv]1602.03049]
- Romeo, A. B. & Wiegert, J. 2011, *MNRAS*, 416, 1191
- Safronov, V. S. 1960, *Annales d'Astrophysique*, 23, 979
- Swartz, D. A., Yukita, M., Tennant, A. F., Soria, R., & Ghosh, K. K. 2006, *ApJ*, 647, 1030
- Tamburro, D., Rix, H.-W., Walter, F., et al. 2008, *AJ*, 136, 2872
- Thornley, M. D. & Mundy, L. G. 1997, *ApJ*, 484, 202
- Toomre, A. 1964, *ApJ*, 139, 1217
- Tremaine, S. & Weinberg, M. D. 1984, *ApJL*, 282, L5
- von Linden, S., Reuter, H.-P., Heidt, J., Wielebinski, R., & Pohl, M. 1996, *A&A*, 315, 52
- Walter, F., Brinks, E., de Blok, W. J. G., et al. 2008, *AJ*, 136, 2563
- Wang, B. & Silk, J. 1994, *ApJ*, 427, 759
- Wilson, C. D., Warren, B. E., Irwin, J., et al. 2011, *MNRAS*, 410, 1409
- Zeilinger, W. W., Vega Beltrán, J. C., Rozas, M., et al. 2001, *Astrophysics and Space Science*, 276, 643
- Zhang, X. & Buta, R. J. 2015, *NewA*, 34, 65

A

Is the short-wavelength approximation satisfied?

To satisfy the short-wavelength approximation, the following statement must hold: $\lambda_3 \ll 2\pi R$. It is remarkable that for the large part of the data, the short-wavelength approximation do hold. However, for a few points in the central regions of some of the galaxies the approximation is definitely invalid. This happens for galaxy NGC 628, NGC 3198, NGC 3521, NGC 4736 and NGC 7331, as can be seen in Fig. A.1.

A. Is the short-wavelength approximation satisfied?

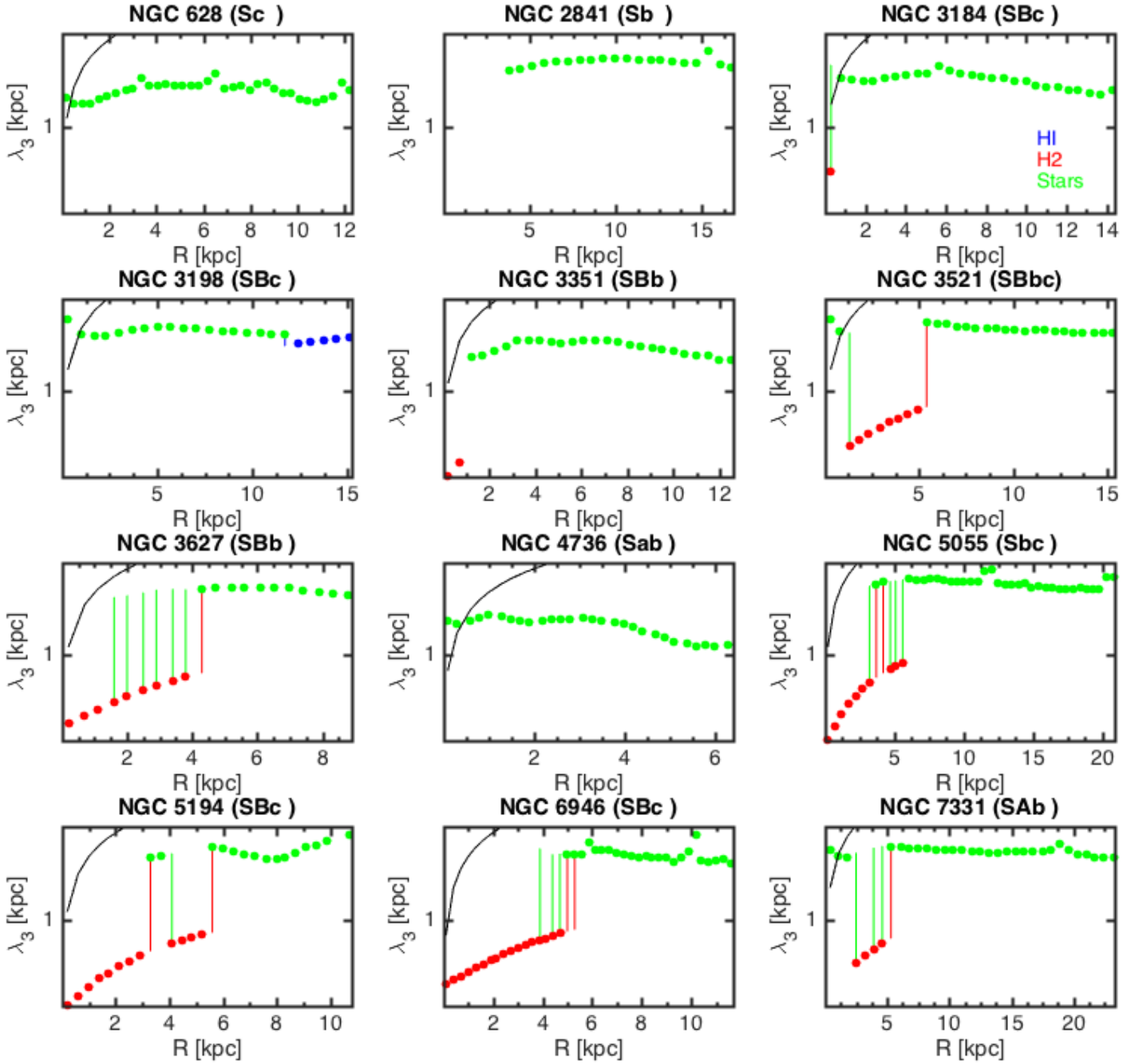


Figure A.1: The figure show the entire sample of the 12 THINGS spiral galaxies. The black line in the top left corner of each graph is the $2\pi R$ -line, below which the short-wavelength approximation is valid. That is, the approximation is valid for $\lambda_3 \ll 2\pi R$.

B

Radial profiles for other spiral galaxies

Due to the reliability of locations of resonances and structures in the sample of 12 spiral galaxies, only five galaxies were chosen for the analysis in Chapter 3.2. The other 7 galaxies included in the paper by Leroy et al. (2008) are: NGC 2841, NGC 3184, NGC 3198, NGC 3521, NGC 4637, NGC 5055 and NGC 5194. The literary background and their radial profiles are presented below.

NGC 2814

A ring and a non-prominent bar is expected to be present in this SA(r)b galaxy. NGC 2841 is located at a distance of 14.1 Mpc. Tamburro et al. (2008) provide the corotation radius of $155''$, using the same inclination and position angle as Leroy et al. (2008). In the data of Leroy et al. (2008) the surface density of H₂ suffer from rather large uncertainties, and several data points are unresolved and unsuitable for a stability analysis.

The radial profiles for the characteristic instability wavelengths and Q stability parameters are displayed in Fig. B.1. As can be seen, the radial extent of the Q stability parameter for molecular gas (top right) ends before the CR, and are subjected to large errors.

NGC 3184

This barred ringed galaxy, i.e SAB(rs)cd, is located at a distance of 11.1 Mpc, and has a corotation radius provided by Tamburro et al. (2008): $127''$, using the same inclination and position angle as Leroy et al. (2008). The radial profiles for the characteristic instability wavelengths and Q stability parameters are displayed in Fig. B.2.

NGC 3198

NGC 3198 (SB(rs)c) is 13.8 Mpc away and contains a bar, as well as ringlike structure of $50''$, according to Corradi et al. (1991). Inside the ring there is a weak bar. The data for a more precise size of this bar is unspecified since it is not prominent. The inclination and position angle are consistent with the values adopted by Leroy et al. (2008), only one degree discrepancy in inclination.

The radial profiles for the characteristic instability wavelengths and Q stability parameters are displayed in Fig. B.3. The Q_{H_2} curve in the top left of Fig. B.3 has some rather interesting form (similar to the shape of Q_{H_2} of NGC 3351, Fig. 3.8), which could yield interesting insights if further studied.

NGC 3521

For this SAB(rs)bc galaxy located at a distance of 10.7 Mpc, Tamburro et al. (2008) provide a corotation radius of $160''$, adopting the same inclination and position angle as Leroy et al. (2008). Zeilinger et al. (2001) found the bar at a radius of $25'' - 45''$, and the ring is expected to be located somewhere outside of that. Zeilinger et al. (2001) have adopted $i = 61^\circ$ and P.A. = 163° , which is a bit off from the values of Leroy et al. (2008) ($i = 73^\circ$ and P.A. = 340°).

The radial profiles for the characteristic instability wavelengths and Q stability parameters are displayed in Fig. B.4, where we can see some rather interesting features in the bottom left graph for the characteristic instability wavelength. NGC 3521 has two transitions between components dominating the instability. The first transition from star-domination to molecular gas is indicated by the minimum radial extent of the bar. The inner star-dominated data points do not satisfy the short-wavelength approximation, as seen in Appendix A though. The second transition does not coincide with any known structure, but the radial extent of the ring is still unknown.

NGC 4736

NGC 4736 is a (R)SA(r)ab galaxy, located at a distance of 4.7 Mpc. From IR and CO observations a bar can be seen of radius $20''$, according to Rand & Wallin (2004). A ring of star formation of radius $45''$ is visible in the $H\alpha$ image, but in CO it corresponds to a pair of tightly wrapped spiral arms. Optical images also reveals a faint outer stellar ring of $5'$. Rand & Wallin (2004) use: $i = 35^\circ$ and P.A. = 295° , compared to Leroy et al. (2008) of $i = 41^\circ$ and P.A. = 296° . Rand & Wallin (2004) go on to explain that NGC 4736 has a non-axisymmetric disk, and the outer ring is located at the OLR of an oval distortion while the starburst ring is located at the ILR of this oval distortion. The OLR of the inner spiral/ring coincides with the ILR of the outer pattern. The spiral/ring is likely to be located at the OLR of the bar. The corotation of the bar is at about 1.3 bar radii, $26''$. Worth noting is that the deprojected bar and oval are neither aligned nor orthogonal and thus cannot be sustained by a single pattern. There are discussions of a different pattern speed, a faster one than the previously used for the outside of the bar. This would place the CR just outside the spiral/ring at $50 - 70''$, the OLR at $70 - 120''$ and one or two ILRs at $20''$. So the ILR of the outer pattern would coincide with the CR of the inner bar, due to the uncertainties it could also be so that it is the inner UHR of the outer pattern that coincides with the CR. The CR of the outer pattern would be located just outside the bright CO emission and star formation. But this would result in no resonance at the location of the outer stellar ring, but this ring could be due to another pattern, a third pattern.

The radial profiles for the characteristic instability wavelengths and Q stability parameters are displayed in Fig. B.5. In the top right graph, the Q_{H_2} curve has a very distinct minimum, which may be related to the ring or the CR of the bar, since they surround the minimum.

NGC 5055

Thornley & Mundy (1997) explain that the central kpc of this SA(rs)bc galaxy shows a nearly axisymmetric distribution of molecular gas while at larger scales

there is a clear non-axisymmetric structure. These deviations are consistent with enhanced gas surface densities along the arms. Thornley & Mundy (1997) continue to describe that at a radius of $40''$, a ring or tight spiral can be seen. The CO velocity field shows no evidence for bar dynamics near the centre, though there is a peak in emission elongated along the major axis over the inner $30''$, perhaps only a peak of the molecular disk. The ILR of the pattern, $30 - 45''$ coincides with the ring and the CR is located somewhere at the edge of the spiral pattern: $120 - 180''$. While Tamburro et al. (2008) provide a corotation radius of the pattern at $264''$, adopting the same inclination and position angle as Leroy et al. (2008): $i = 59^\circ$ and P.A = 102° . Thornley & Mundy (1997) use $i = 64^\circ$ and P.A = 101° , and the distance adopted to this galaxy is 10.1 Mpc.

This galaxy has some rather interesting radial profiles. The radial profiles for the characteristic instability wavelengths and Q stability parameters are displayed in Fig. B.6, where we can see three transitions between the two components that dominate the instability (though the first two domination-transitions are located in a region of large errorbars). The third transition, the one from H2- to star-domination, is close to the minimum radial extent of the CR, but note that the CR derived by Tamburro et al. (2008) is far to the right, the uncertainties are large.

NGC 5194

This is a strongly interacting SA(s)bc peculiarly shaped galaxy, also called the Whirlpool galaxy, located at a distance of 8 Mpc. Meidt et al. (2011) state that there are three different pattern speeds, two of them are located within a radial distance of $89''$. The transition between the two pattern speeds appear to occur at a resonance overlap, perhaps it is the CR of pattern 1 that overlaps with the UHR of pattern 2, at $43''$. This is most likely where a transfer of energy between bar and spiral occurs. The third pattern is hard to pinpoint in simulations and observations, and it is therefore not a part of the analysis by Meidt et al. (2011). Meidt et al. (2011) use $i = 24 \pm 3^\circ$ and P.A = $170 \pm 5^\circ$, not a very large discrepancy compared to the values adopted by Leroy et al. (2008): $i = 20^\circ$ and P.A = 172° . For this galaxy Tamburro et al. (2008) provide a corotation radius of $116.76''$, using: $i = 42^\circ$ and P.A = 172° . The difference of more than 20 degrees in inclination could show effects in the calculations and simulations.

The radial profiles for the characteristic instability wavelengths and Q stability parameters are displayed in Fig. B.7. If we begin by looking at the bottom left graph of the three-component characteristic instability wavelength, we can see three transitions between the two dominating components. The location of the first few points that are dominated by stars, $3.2 - 4\text{kpc}$, are located at a region of lower surface density of molecular gas than the surroundings, and the first transition (closest to the centre of the galaxy) coincides with the CR of the second pattern. From the Q stability graphs (the top two graphs in Fig. B.7) it is possible to draw the conclusion of an interacting galaxy. There are interesting features and movements in this galaxy, which definitely are worth further and more extensive studies.

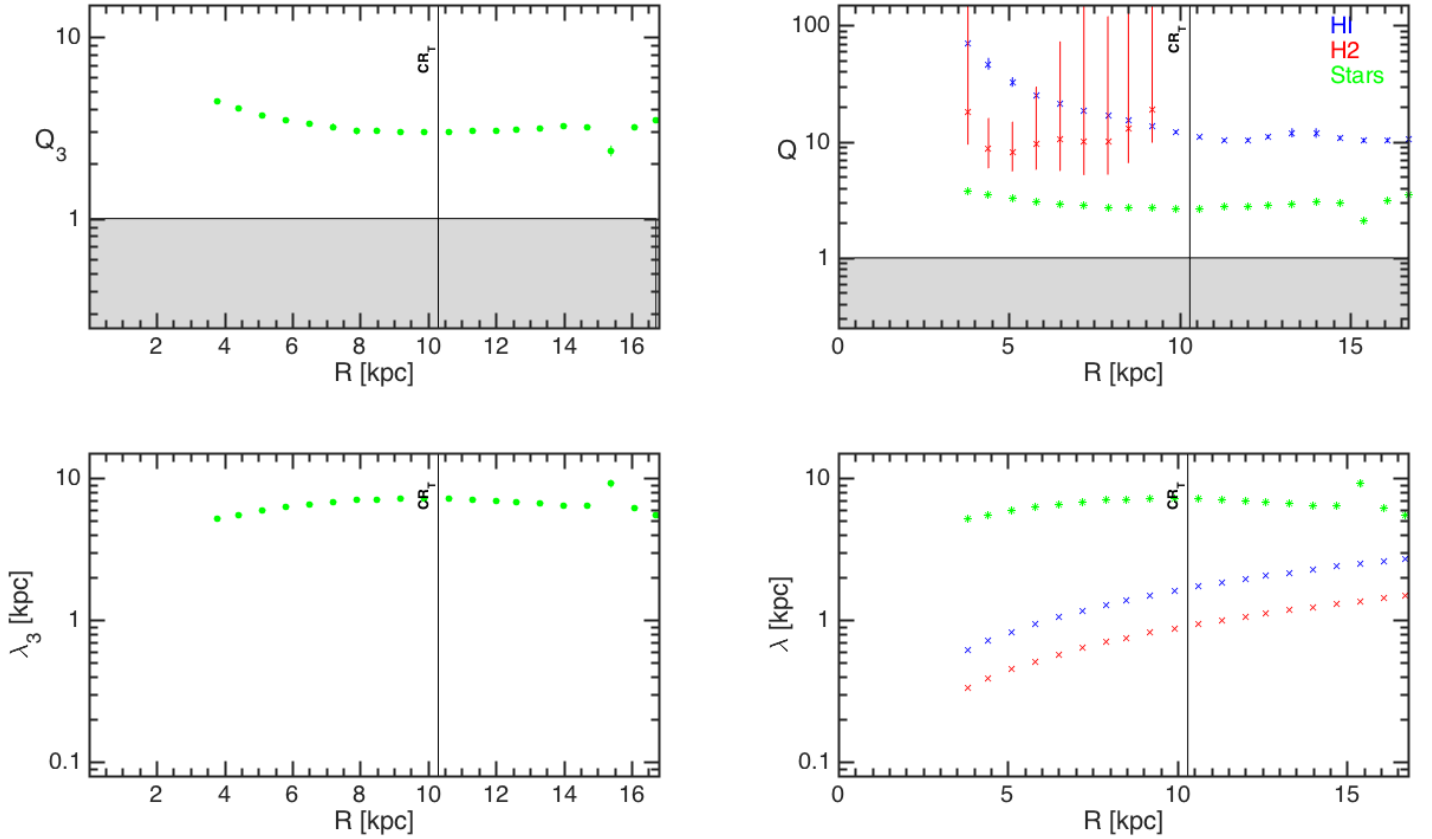


Figure B.1: Radial profiles for NGC 2841 (SA(r)b); The three component Romeo-Falstad Q stability parameter (top left), the classical Toomre parameter for each component (top right), the three component characteristic instability wavelength (bottom left) and the characteristic instability wavelength for the individual components (bottom right). The vertical lines indicate the radial extents of the structural features in NGC 2841. The vertical line is labelled CR_T (the CR of Tamburro et al. (2008)).

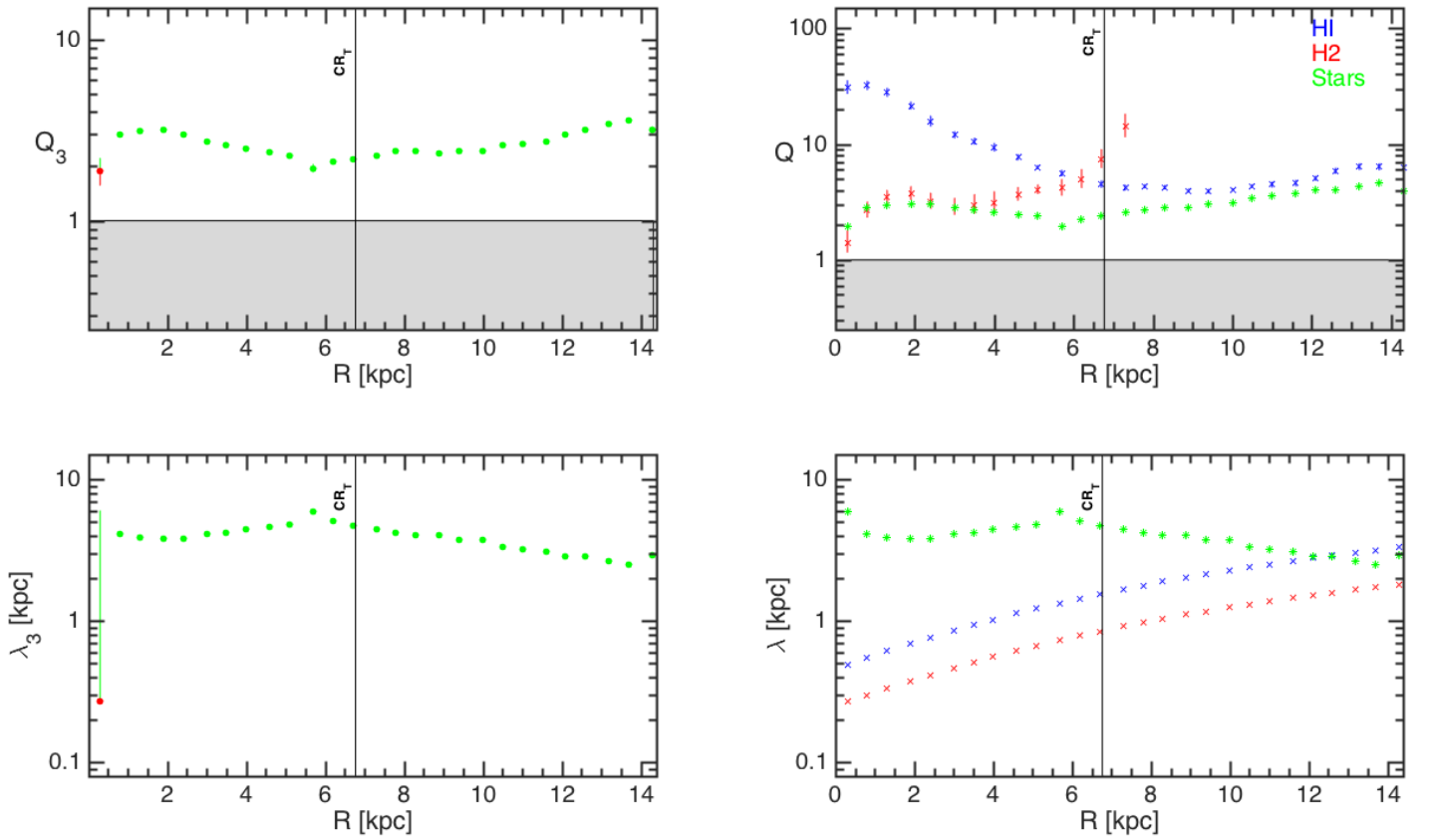


Figure B.2: Same as Fig. B.1 but for NGC 3184 (SAB(rs)cd). The vertical lines indicate the radial extents of the structural features in NGC 3184. The vertical line is labelled CR_T (the CR of Tamburro et al. (2008)).

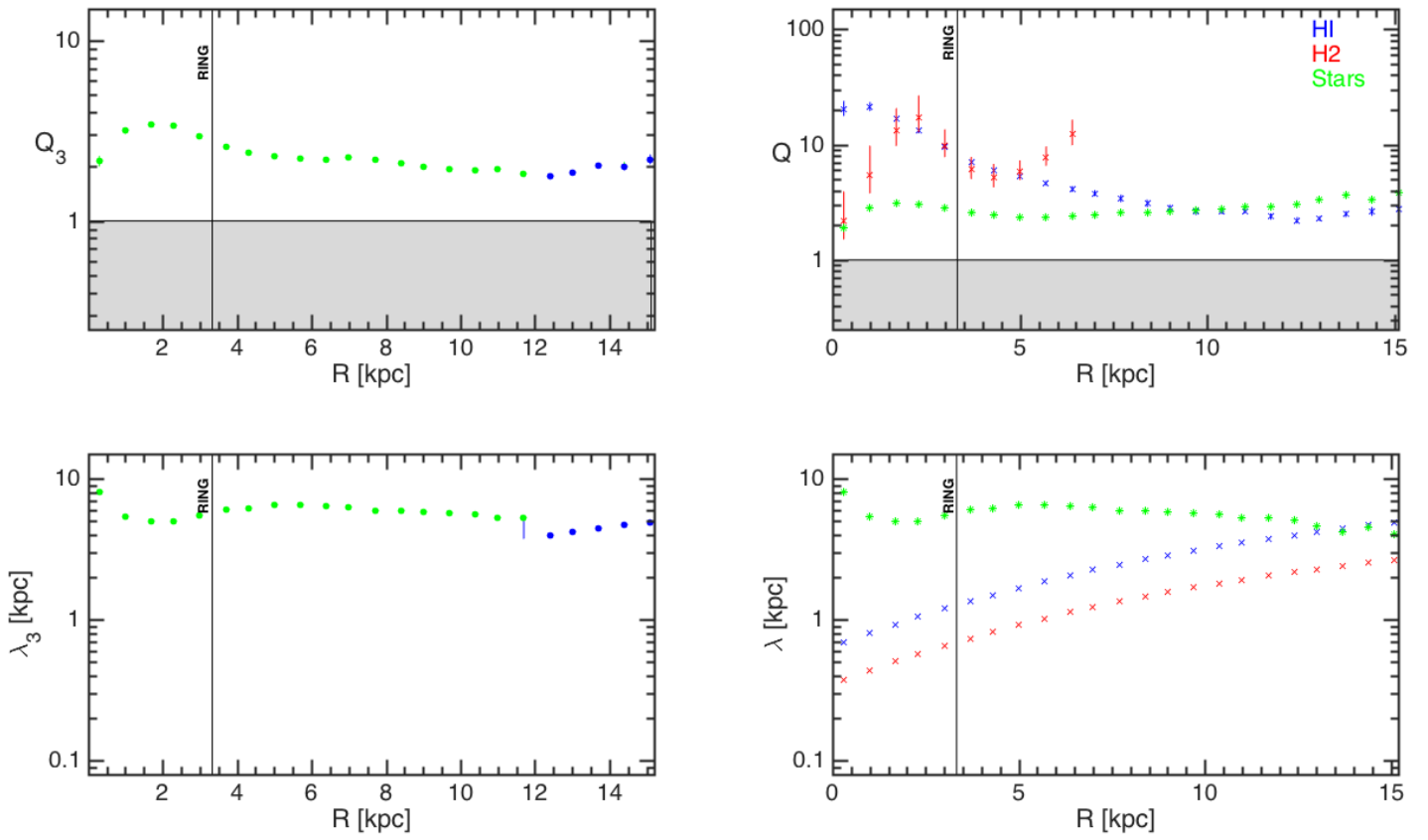


Figure B.3: Same as Fig. 3.7 but for NGC 3198 (SB(rs)). The vertical line is labelled RING.

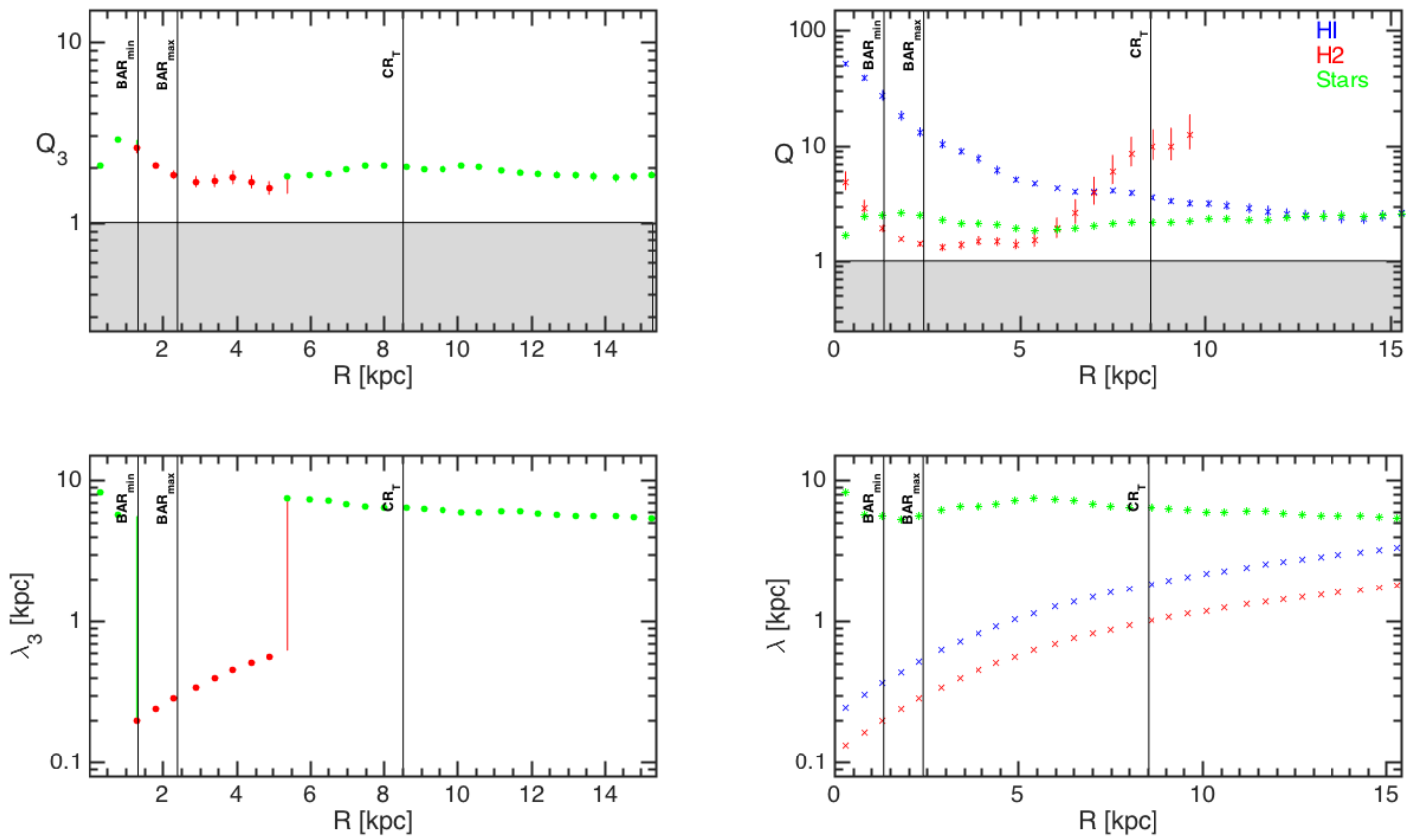


Figure B.4: Same as Fig. 3.7 but for NGC 3521 (SAB(rs)bc). The vertical lines are labelled, from left to right, as: BAR_{min} , BAR_{max} , CR_T (the CR of Tamburro et al. (2008)).

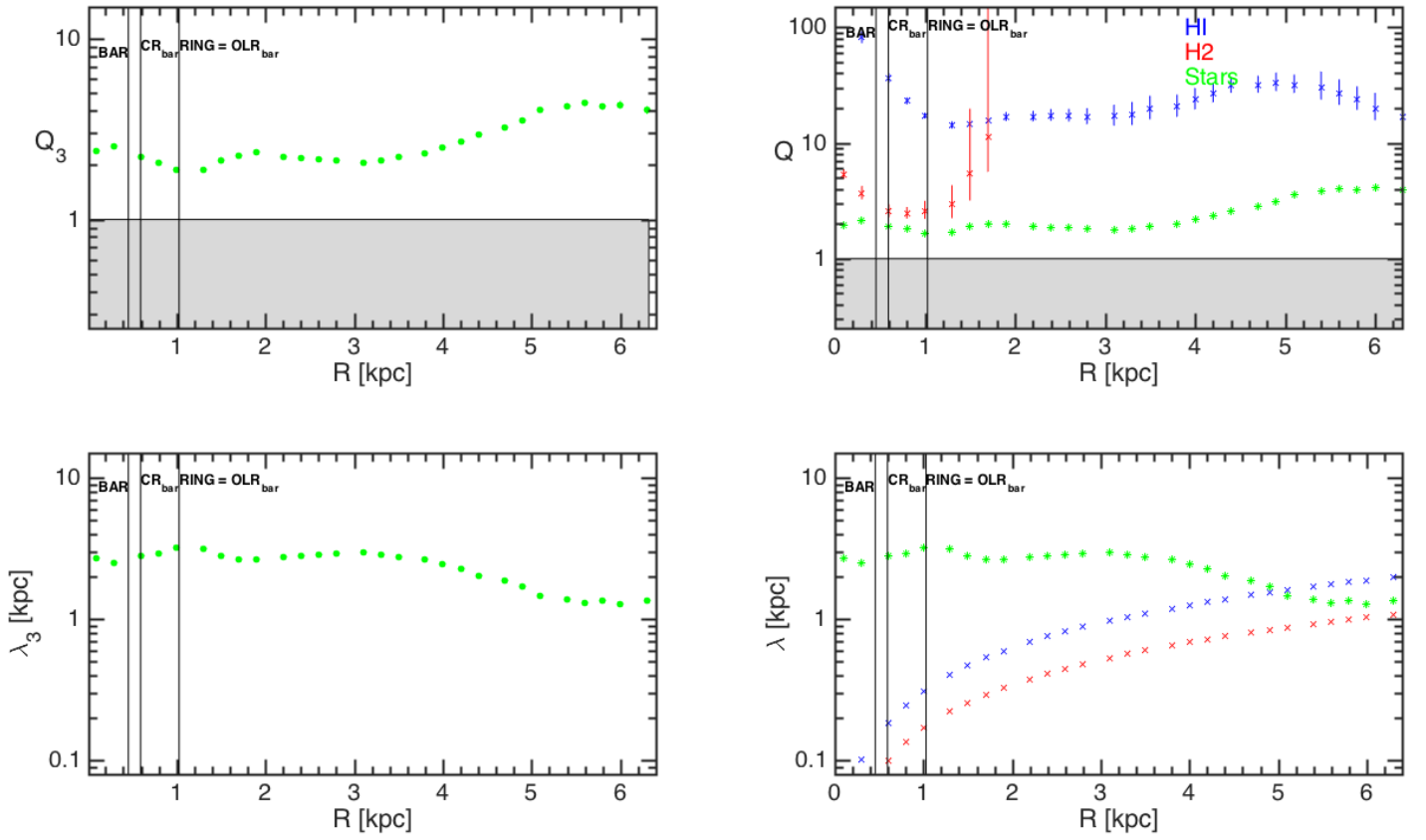


Figure B.5: Same as Fig. 3.7 but for NGC 4736 ((R)SA(r)ab). The vertical lines are labelled, from left to right, as: BAR, RING, CR_{bar} , RING = OLR_{bar} .

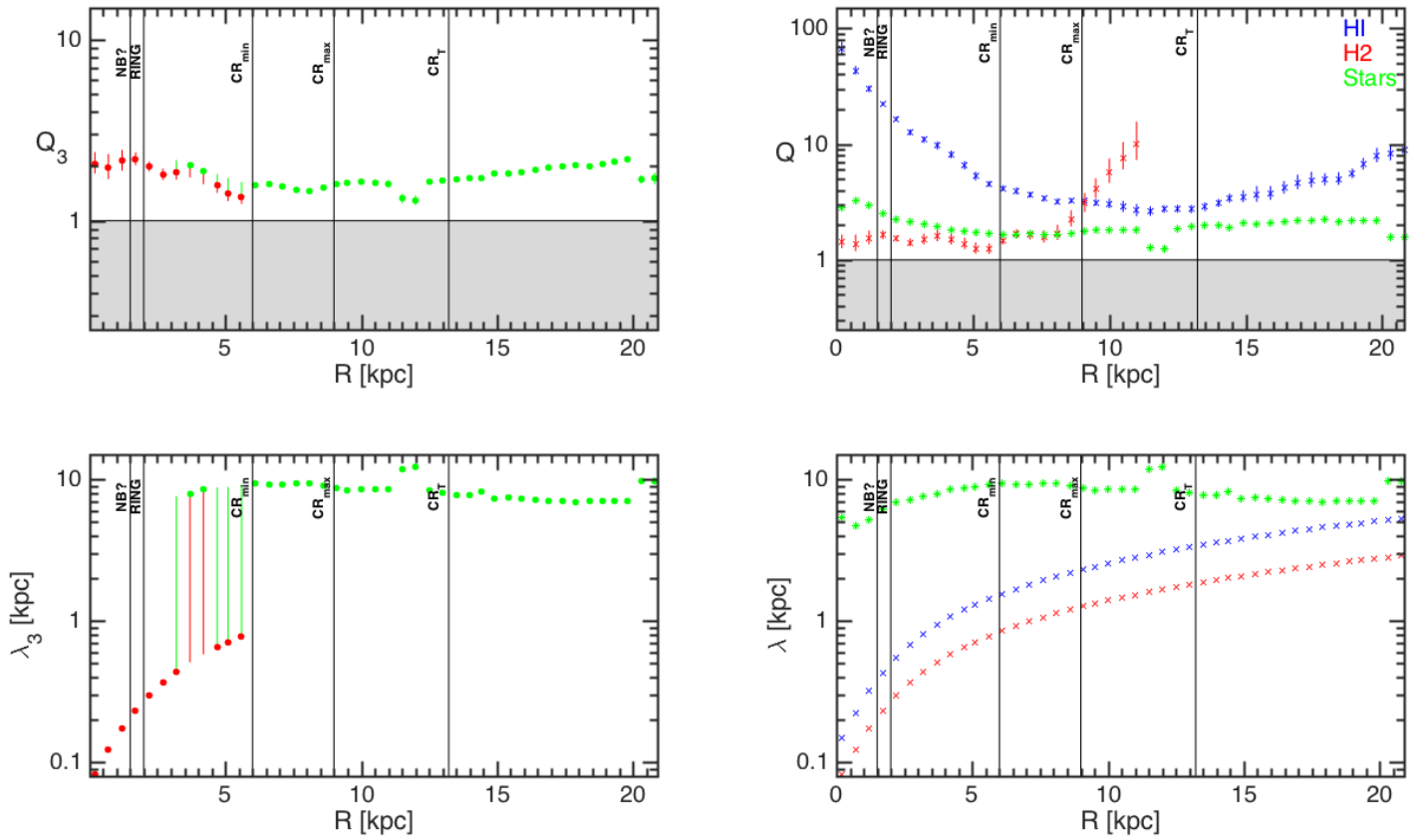


Figure B.6: Same as Fig. 3.7 but for NGC 5055 (SA(rs)bc). The vertical lines are labelled, from left to right, as: NB?, RING, CR_{min} , CR_{max} , CR_T (the CR of Tamburro et al. (2008)).

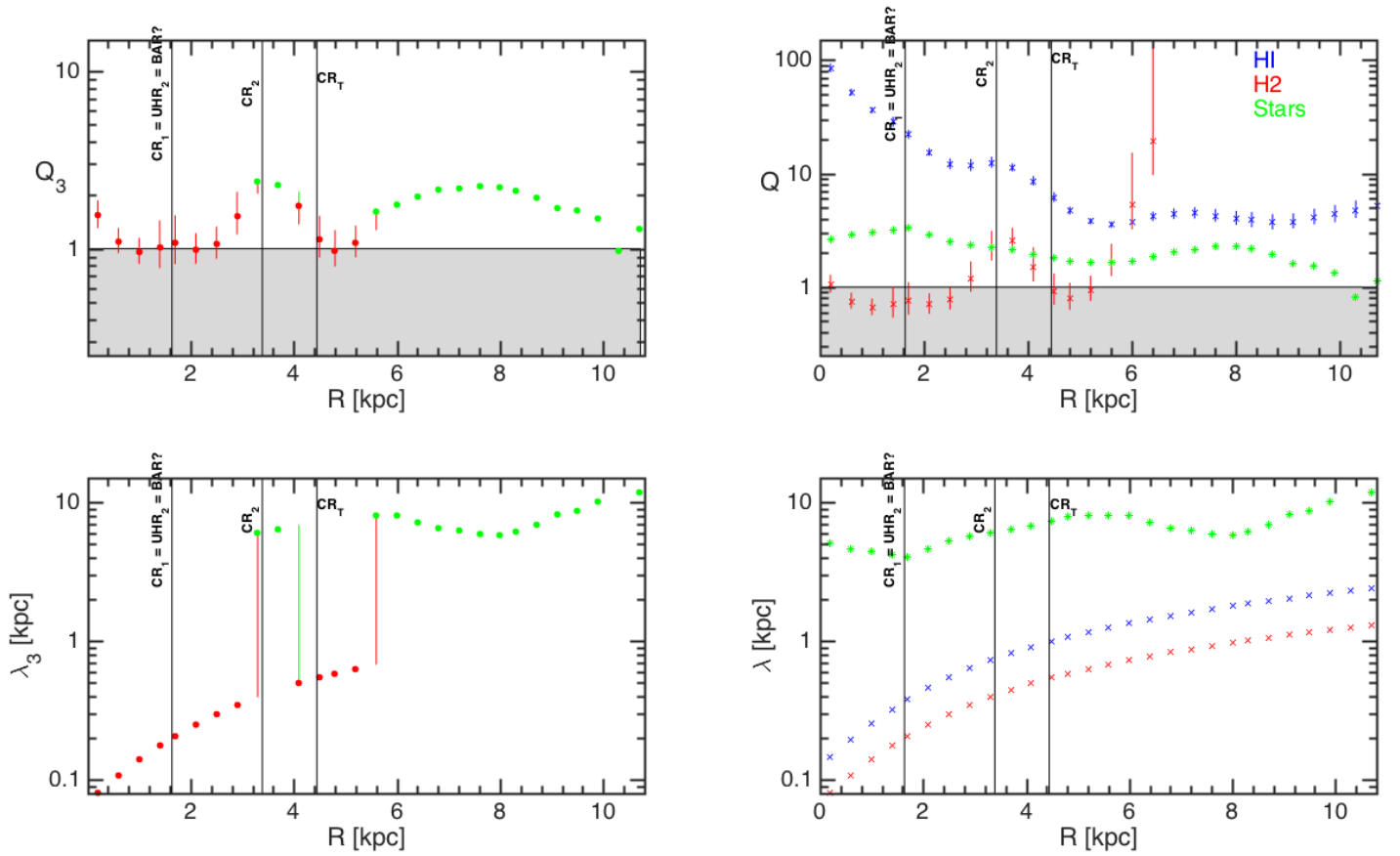


Figure B.7: Same as Fig. 3.7 but for NGC 5194 (SA(s)bc). The vertical lines are labelled, from left to right, as: $CR_1? = UHR_2 = BAR?$, CR_2 , CR_T (the CR of Tamburro et al. (2008)).